Damage characterization of laminated composites using acoustic emission: A review

Saeedifar, Milad; Zarouchas, Dimitrios

DOI
10.1016/j.compositesb.2020.108039

Publication date
2020

Document Version
Final published version

Published in
Composites Part B: Engineering

Composites Part B 195 (2020) 108039

Contents lists available at ScienceDirect

Composites Part B

journal homepage: www.elsevier.com/locate/compositesb

Damage characterization of laminated composites using acoustic emission: A review

Milad Saeedifar, Dimitrios Zarouchas *

Structural Integrity & Composites Group, Delft University of Technology, the Netherlands

ARTICLE INFO

Keywords:
Acoustic emission
Laminated composites
Damage characterization
Damage diagnostics
Damage prognostics

ABSTRACT

Damage characterization of laminated composites has been thoroughly studied the last decades where researchers developed several damage models, and in combination with experimental evidence, contributed to better understanding of the structural behavior of these structures. Experimental techniques played an essential role on this progress and among the techniques that were utilized, acoustic emission (AE) was extensively used due to its advantages for in-situ damage monitoring with high sensitivity and its capability to inspect continuously a relatively large area. This paper presents a comprehensive review on the use of AE for damage characterization in laminated composites. The review is divided into two sections; the first section discusses the literature for damage diagnostics and it is presented in three subsections: damage initiation detection, damage type identification and damage localization, while the second section is devoted to damage prognostics and it focuses on the remaining useful life (RUL) and residual strength prediction of composite structures using AE data. In every section, efforts have been made to analyze the most relevant literature, discuss in a critical manner the results and conclusions, and identify possibilities for future work.

1. Introduction

Laminated composite structures, driven by advantages in structural efficiency, performance, versatility and cost, have made a significant mark in numerous industries, such as aerospace, wind energy, automotive and naval. However, their full potential is held back by an overall lack of understanding of the damage accumulation process over the lifetime of the structure. It is yet unclear how different damage mechanisms are triggered, which parameters and how they affect their interaction, and what is the precise influence of a particular damage state on the integrity of structural component. As a consequence, large safety factors must be applied in composite design to compensate for this deficiency in understanding. The overdesign due to these large safety factors reduces the potential efficiency of composite structures, particularly in terms of their weight.

In general, the damage mechanisms in laminated composites are categorized into two groups: interlaminar and intralaminar damage mechanisms. Delamination is an interlaminar damage mechanism, which is defined as the initiation and propagation of an interlaminar matrix crack that leads to the separation of two laminas and significantly degrades the out-of-plane and flexural properties and of the composite structure [1–3]. The intralaminar damage mechanisms refer to damages within a lamina, i.e. matrix cracking, fiber breakage, fiber/matrix debonding and fiber pull-out [4–7].

The damage accumulation sequence depends on many variables such as the material properties of the composite's constituents, the exact layup, the defects induced during manufacturing, the loading profile and the environmental conditions in which the structure operates. Additionally, the inhomogeneous nature of the composite material and the stochastic activation of different damage mechanisms should also be taken into account making the damage process a very complex phenomenon to study.

In the effort to unfold the damage accumulation process, researchers have employed several experimental techniques. Extensive research has been performed the last three decades in the field of damage assessment using experimental techniques and as a result a large amount of sensing technologies exist nowadays [8–17]. These techniques are generally categorized into two main groups: active techniques and passive techniques. In the case of active techniques, the composite structure is excited by a foreign source. Then, according to the response of the excited structure, the damage is identified. The most common active techniques used for damage assessment in the laminated composites are ultrasonic inspection [18,19], active thermography [20–22], modal

* Corresponding author.
E-mail address: d.zarouchas@tudelft.nl (D. Zarouchas).

https://doi.org/10.1016/j.compositesb.2020.108039
Received 1 December 2019; Received in revised form 27 January 2020; Accepted 3 April 2020
Available online 25 April 2020

Abbreviations

AE	Acoustic emission
aJ	Attojoule
ANN	Artificial neural network
BNN	Bayesian neural networks
CAI	Compression after impact
CFRP	Carbon fiber reinforced polymer
DCB	Double cantilever beam
DIC	Digital image correlation
ENF	End-notched flexural
FCM	Fuzzy c-means
FFT	Fast Fourier transform
GFRP	Glass fiber reinforced polymer
GKM	Genetic k-means
GMD	Gaussian mixture distribution
HDT	Hit definition time
HT	Hilbert transform
LVI	Low-velocity impact
MARSE	Measured area under the rectified signal envelope
MMB	Mixed-mode bending
NHHSMM	Nonhomogeneous hidden semi Markov model
OHT	Open-hole tensile
PCA	Principal component analysis
PDT	Peak definition time
RA	Rise time/amplitude
RUL	Remaining useful life
SEM	Scanning electron microscope
SHM	Structural health monitoring
SOM	Self-organizing map
SVM	Support vector machine
UHMWPE/HDPE	Ultra high molecular weight polyethylene fiber reinforced high-density polyethylene
WT	Wavelet transform
3 PB	3-point bending
4 PB	4-point bending

analysis [23,24], eddy current [25], radiography [26], guided wave [27,28], terahertz imaging [29] and shearography [30,31]. The weakness of the active SHM techniques is the fact that they are not capable of online monitoring of the composite structures in operation [32]. In the case of passive techniques, there is not any foreign source to excite the material and the sources are inside the material. These sources may be damage nucleation, damage propagation, plastic deformation, internal friction, etc. The most common passive techniques are acoustic emission (AE) and passive thermography [33]. The superiority of the passive techniques over the active ones is their capability for structural health monitoring (SHM) while the structure is in operation.

This review paper discusses the advantages of AE, which has the potential to be used for SHM. SHM can be described as the process of implementing a real-time damage detection strategy for load bearing structures. This process involves the observation of the mechanical response and the integrity assessment of the structure by using permanently installed sensors. The sensors record data periodically or continuously over the in-service life of the structure. The sensors cannot measure damage but the response of the structure. Thus, the sensitive information is hidden within the data, and feature extraction using advanced data analytics should be performed in order to relate the observations with the damage states. The main target of the feature extraction is to fulfil the four SHM levels; 1) damage detection, 2) damage localization, 3) damage identification and 4) damage severity.

2. AE as an online damage monitoring tool

The literature review shows AE has been widely used for damage assessment in laminated composites. The first papers on this topic, indexed in Scopus, are referred to the two conference papers authored by Hagemaier et al. [34,35] in the 1970s. They used AE to detect material and manufacturing anomalies in graphite composites. As depicted in Fig. 1, since the 1970s, there is an increasing trend to use AE for damage analysis and assessment of composite materials, especially during the last decade. During these five decades, around 700 papers have been published on this topic, including ~450 journal papers and ~250 conference papers. This data was obtained from Scopus (23 October 2019) using the keywords: acoustic emission and composite laminate.

AE is defined as the transmission of an elastic stress wave through the

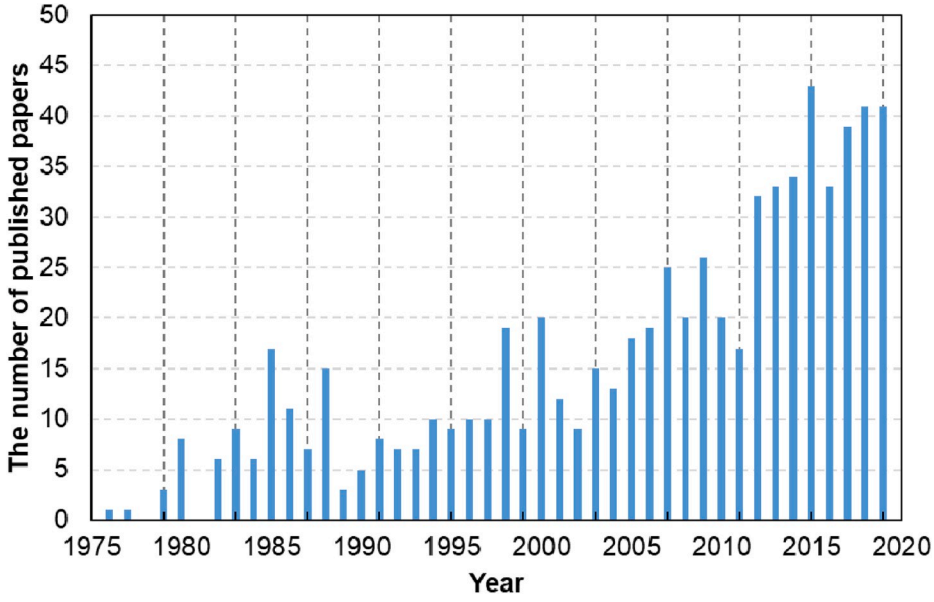

Fig. 1. The number of indexed papers in Scopus (23 October 2019) using the keywords: acoustic emission and composite laminate.

material which is usually originated from an internal source such as crack initiation and growth [32]. According to Fig. 2, the required apparatus to perform AE monitoring consists of:

- The structure under loading.
- A network of AE sensors to capture the infinitesimal surface vibrations of the test structure and to convert them to the analog signals.
- Pre-amplifiers which magnify the intensity of the analog signals.
- Acquisition and recording section, where the amplified signals are recorded and converted from the analog to digital signals.
- Data processing section, where the recorded digital AE waveforms are analyzed.

The AE analyses are usually performed using AE waveforms or the features extracted from the AE waveforms. Fig. 3 shows a typical AE waveform. The most important features of an AE waveform are the following:

- Threshold: Only the AE signals with the intensity higher than the threshold are recorded by the AE system. It is reported in dB unit.
- Amplitude: The maximum voltage of the signal and it is usually reported in dB unit.
- Duration: The time interval between the first and the last threshold crossings and it is reported in μs unit.
- Rise time: The time interval between the first threshold crossing and the maximum amplitude and it is reported in μs unit.
- Counts: The number that the waveform crosses the threshold in the increasing direction within the waveform's duration.
- Energy: The area beneath the squared waveform within the waveform's duration. It is usually reported in attojoule (aJ) unit (1 aJ = 10^{-18} J).
- Peak frequency: The frequency corresponded to the highest magnitude in the frequency distribution obtained from fast Fourier transform (FFT) of the signal. It is reported in kHz unit.

The published papers in the field of damage characterization of laminated composites using AE can be categorized into two main groups: damage diagnostics and damage prognostics. The first group consists of three subgroups: damage initiation detection, damage localization and damage identification. The second group contains the studies related to the remaining useful life (RUL) and residual strength prediction of composite structures using AE. Accordingly, the literature is presented hereafter in the aforementioned structure where the most relevant papers in the field, the results and conclusions, as well as possibilities for future work are presented and discussed. It is worth to notice that Romhány et al. published recently a review paper on the damage localization in laminated composites using AE [37]. Our review paper does not address the damage localization topic, therefore it is recommended that the reader refers to their work.

3. Damage diagnostics

The procedure of damage diagnosis using AE consists of three levels; damage initiation detection, damage localization and damage identification. The first level deals with the definition of the damage initiation criteria, irrespective of the damage type. Then, in the second level, the damage is localized using a network of AE sensors and different localization methods. Finally, the damage is identified by analyzing the AE data using unsupervised clustering, supervised classification and signal analysis methods.

3.1. Damage initiation detection

Many researchers used AE to detect the initiation of the damage in laminated composites. The studies cover a variety of loading conditions and specimen configurations; from coupon level tests such as tensile, compression, double cantilever beam (DCB), end-notched flexural (ENF), mixed-mode bending (MMB), 3-point bending (3 PB), 4-point bending (4 PB), buckling, quasi-static transverse indentation, low-velocity impact (LVI) and compression after impact (CAI), to a real composite structure subjected to an arbitrary load. The list of literature of damage initiation detection in laminated composites is reported in Table 1. The studies cover a wide range of the composite materials, including thermoset material; glass/epoxy and carbon/epoxy,

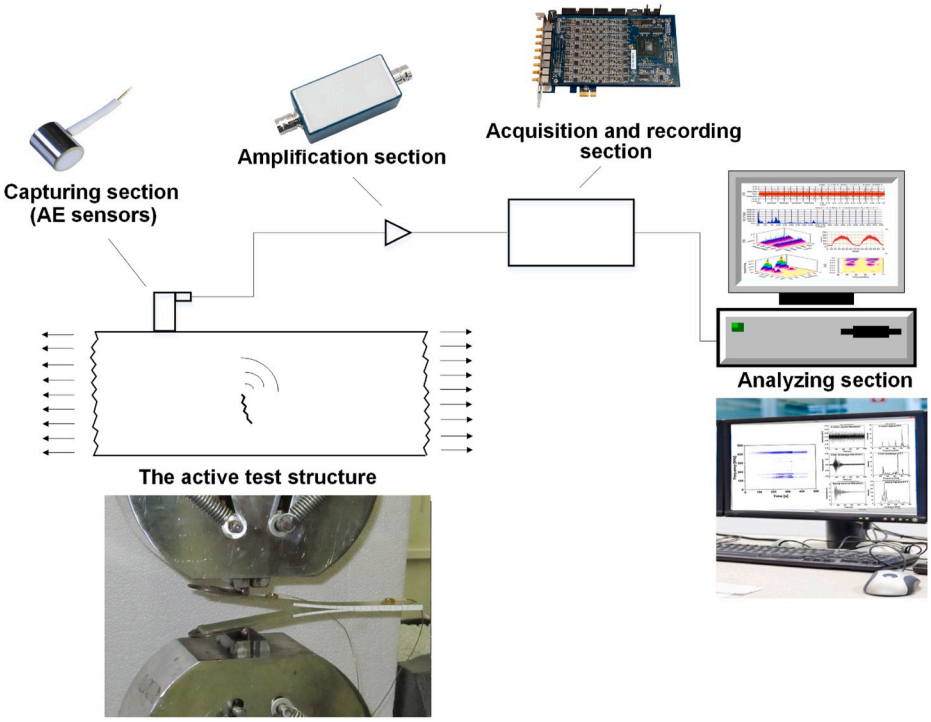

Fig. 2. The different units of an AE monitoring system.

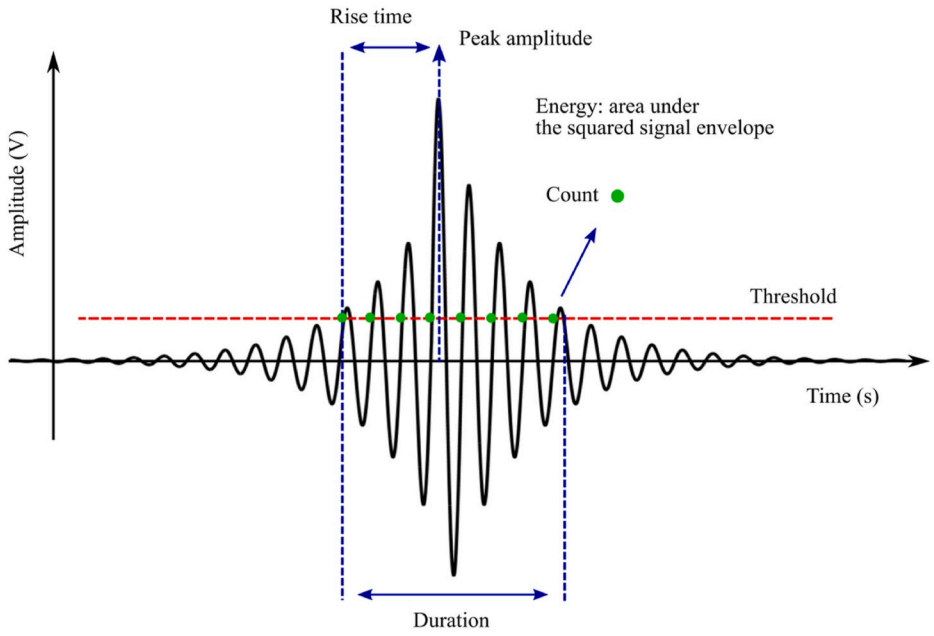

Fig. 3. A typical AE waveform and the most important features [36].

thermoplastic material; glass/polyester and glass/polyamide, sandwich and hybrid composites.

As presented in Table 1, most of the researchers used either one or multiple AE features or a combination of AE features with the mechanical data for identifying the initiation of damage in the material. AE events, AE energy, AE counts and also the cumulative values of these parameters are the main utilized features. In the case where AE events were used as a criterion, the first identified AE event during the loading is considered as the moment of the damage initiation [38,39]. On the other hand, in few papers the first high-energy or high-counts AE signals are used as the criterion for damage initiation [40–42]. Furthermore, there are some studies that used the cumulative AE events, cumulative AE energy, and cumulative AE counts as criterion. The first significant increase in the gradient of these cumulative curves is considered to be the moment of damage initiation [5,6,43,44]. The last group of the researchers tried to increase the sensitivity of damage detection by combining the AE data and the mechanical data by introducing the sentry function [2,45,46]. The sentry function is defined as the logarithm of mechanical energy to the AE energy [47]:

$$f(x) = \ln\left[\frac{E_m(x)}{E_{AE}(x)}\right] \tag{1}$$

where E_m (x) is the mechanical energy (area under the load-displacement curve), E_{AE} (x) is the cumulative AE energy and x is the displacement.

Based on the state of the damage in the structure, the sentry function could show one of the four following trends: 1) Increasing trend: it shows that the structure is still intact and no damage or some micro damages occurred in the material. 2) Sharp drop: it reveals that huge damage occurred in the material. 3) Constant trend: It demonstrates that there is a balance between the degrading mechanisms, like damages, and the strengthening mechanisms, like fiber bridging. 4) Gradually decreasing: It is emphasizing that the load-carrying capability of the composite structure is losing gradually. Accordingly, the first big drop in the sentry function curve is considered as the moment of the damage initiation.

Although different approaches have been proposed for AE-based detection of damage initiation in laminated composites, this task still remains open with challenges to be addressed. The limitations of each proposed method are discussed hereafter. If the first AE event is considered as the moment of the damage initiation, it may lead to conservative indication on when the damage initiated. AE is very sensitive to micro damages while most of these micro damages do not degrade the integrity of the composite structure significantly. For example, a lot of imperfections might be induced in the laminated composite structures during the fabrication process, such as the fiber misalignment, micro voids and impurities [48]. These imperfections could induce many AE events in the early stage of the loading while the structure retains its integrity.

In addition, some of these imperfections could induce high-energy and high-counts AE events. The misalignment of a few numbers of fibers, which frequently happens in the hand layup fabrication process, results in the breakage of the misaligned fibers in the early stage of the loading. Thus, observing the first high-energy or high-counts AE event is not always a reliable indicator of the damage initiation.

Further, the criteria such as “high-energy”, “high-counts”, “the first significant increase” in the gradient of cumulative curves and “the first significant drop” in the sentry function curve are qualitative criteria that can be interpreted in different ways (see Fig. 4).

The possibility of different interpretations of the proposed qualitative criteria to detect the damage initiation in a glass/epoxy DCB test, performed by the authors, is demonstrated in Fig. 4. According to Fig. 4 (a) and in agreement with the aforementioned explanations, considering the first recorded AE event as the sign of the damage initiation, leads to the conservative prediction of damage in the initial loading stages (displacement = 1.45 mm). As it is clearly seen, no degradation is seen in the load curve and load increases up to 3.6 times after detecting the first AE event. In addition, the continuous AE activity initiates at the displacement of 5.6 mm, which is long after the first captured AE event. In Fig. 4(b), AE energy is used to detect the damage initiation. The selection of the first high-energy AE event depends on the scale of the AE energy plot and also the interpretation of the person who is performing the AE data analysis. If the AE energy is plotted in the scale of the maximum recorded energy (around 4300 aJ) the first high energy AE event is detected at the displacement of 43.3 mm which is long after the first load drop. In addition, if the AE energy curve is shown in a magnified view (the upper limit of the AE energy axis -the right vertical axis-is 200 aJ), there are 7 peaks in the AE energy plot with the corresponding displacements of 4.8, 6.6, 8.1, 9.5, 9.9, 10.8 and 13.9 mm, respectively. Based on the user’s judgment and experience, each one

Table 1
Damage initiation detection in laminated composites using AE.

Materials	Type of the test	Damage modes	The utilized AE parameters	Damage detection approach	Ref.
Damage initiation detection by one instantaneous AE feature					
Aluminum to aluminum adhesively-bonded	Quasi-static and fatigue DCB tests	Micro cracks at adhesive bond	Events	Detecting first micro cracks at the adhesive layer before macroscopic delamination failure by first AE events	[39]
Carbon/epoxy	Constant and cyclic internal pressure on the pressure vessel	Fiber breakage	Events	The first AE event	[38]
Glass/polyester	DCB	Delamination	Energy	The first high-energy AE event	[42]
Glass/epoxy	DCB, ENF and MMB	Delamination	Energy	The first high-energy AE event	[41]
Glass/epoxy	3 PB	Delamination	Counts	The first high-counts AE event	[53]
Glass/epoxy	3 PB	Delamination	Counts	The first high-counts AE event	[40]
Sandwich composite with glass/epoxy skin and foam core	DCB	Delamination	Counts	The first high-counts AE event	[54]
Damage initiation detection by cumulative curve of AE features					
Glass/epoxy	Quasi-static indentation	Matrix cracking, delamination and fiber breakage	Cumulative energy	Different damage mechanisms were clustered using packet wavelet transform and cumulative energy used to detect the initiation of each damage mechanism	[55]
Carbon/epoxy	DCB	Delamination	Cumulative energy	The first increase in the gradient of cumulative energy curve	[43]
Glass/epoxy	ENF	Matrix cracking, fiber/matrix debonding and fiber breakage	Cumulative energy	The signals were clustered using FCM, then the first increase in the gradient of cumulative energy curve for each damage was considered as the initiation of that damage mode	[7]
Carbon/epoxy	DCB fatigue	Delamination	Cumulative energy	By fitting a linear equation to the cumulative energy and delamination growth data, crack growth was predicted by AE	[56]
Glass/epoxy	Tensile	Layer failure and delamination	Cumulative energy	The first increase in the gradient of cumulative energy curve	[57]
Glass/epoxy	DCB	Delamination	Cumulative energy	By fitting a linear equation to the cumulative energy and delamination growth data, crack growth was predicted by AE	[58]
Carbon/epoxy	Quasi-static indentation	Matrix cracking, delamination and fiber breakage	Cumulative energy and cumulative events	The signals were clustered by the hierarchical model, then first increase in the gradient of cumulative events and cumulative energy curves showed the damage initiation	[5]
Glass/polyamide	Fatigue tensile	Matrix cracking, delamination and fiber breakage	Cumulative events	The signals were clustered according to their amplitude, then the first increase in the gradient of cumulative events curve, for each damage, was considered as the initiation of that damage mode	[6]
Glass/epoxy	Quasi-static and fatigue tensile tests	Matrix cracking, fiber/matrix debonding, delamination and fiber breakage	Cumulative events	The signals were clustered using an unsupervised clustering method, then the first increase in the gradient of cumulative events curve, for each damage, was considered as the initiation of that damage mode	[4]
Glass/epoxy	DCB	Matrix cracking, fiber/matrix debonding and fiber breakage	Cumulative counts	The signals were clustered by Hilbert transform (HT), then the first increase in the gradient of cumulative counts curve, for each damage, was considered as the initiation of that damage mode	[44]
Glass/epoxy	Tensile test of the drilled specimen	Matrix cracking	Cumulative counts	The first increase in the gradient of cumulative counts curve	[59]
Glass/epoxy	ENF	Delamination	Cumulative counts	The first increase in the gradient of cumulative energy curve	[60]
Sandwich composite with glass/epoxy skin and foam core	DCB	Interfacial debonding, matrix cracking, fiber breakage and core failure	Cumulative counts	Different damage mechanisms were clustered using GKM algorithm and cumulative counts was utilized to detect the initiation of each damage mechanism	[61]
Damage initiation detection by the combination of AE and mechanical data					
Sandwich composite with glass/epoxy skin and foam core	DCB	Delamination	Sentry function	The transition point in the plot of the integration of sentry function against cumulative energy release rate	[62]
Glass/epoxy	DCB	Delamination	Sentry function	The first significant drop in the sentry function curve	[63]
Glass/polyester	DCB	Delamination	Sentry function	The first significant drop in the sentry function curve, the transition point in the plot of the integration of sentry function against cumulative energy release rate	[46]
Carbon/epoxy	DCB, ENF and MMB	Delamination	Sentry function	The first significant drop in the sentry function curve	[2]
Damage initiation detection by several approaches					
Hybrid of thin carbon/epoxy and conventional glass/epoxy	Tensile	Fiber fracture and ply fragmentation	Energy and cumulative energy	The first high-energy signal, the first significant increase in the gradient of cumulative energy curve	[64]
Carbon/Thermoset resin Carbon/Thermoplastic resin	DCB	Delamination	Events, cumulative energy and cumulative events	The first increase in the gradient of cumulative energy curve, the first increase in the number of AE events, the first increase in the gradient of cumulative events curve	[65]
Hemp/epoxy Glass/epoxy	3 PB	Global collapse			[66]

(*continued on next page*)

Table 1 (*continued*)

			Events, normalized cumulative counts and normalized counts rate	The first AE event, the first increase in the gradient of normalized cumulative counts curve and the first high-counts rate event	
Glass/epoxy	DCB, ENF and MMB	Delamination	Cumulative energy, energy rate and sentry function	The first high-energy AE event, the first increase in the gradient of cumulative energy curve and the first significant drop in the sentry function curve	[67]
Glass/epoxy	ENF	Delamination	Counts, energy and sentry function	The first high-counts AE event and the first significant drop in the sentry function curve	[68]
Glass/epoxy	DCB	Delamination	Counts, energy and sentry function	The first high-counts AE event and the first significant drop in the sentry function curve	[69]
Glass/epoxy	ENF	Delamination	Energy and sentry function	The first high-counts AE event and the first significant drop in the sentry function curve	[70]
Glass/epoxy	DCB	Delamination	Energy and sentry function	The first high-energy AE event and the first significant drop in the sentry function curve	[1]
Glass/epoxy	DCB, ENF and MMB	Delamination	Energy, cumulative energy and sentry function	The first high-energy AE event, the first increase in the gradient of cumulative energy curve and the first significant drop in the sentry function curve	[3]
Glass/epoxy	Buckling	Delamination	Energy, cumulative counts and sentry function	The first high-energy AE event, the first increase in the gradient of cumulative counts curve and the first significant drop in the sentry function curve	[71]

could be considered as "the first high-energy AE event" and therefore damage initiation. A similar problem exists if AE counts are used for damage indicator. Therefore, the obtained results depend on the plot scale and also the operator's interpretation. Similar to the previous approaches, in the case of cumulative AE energy, cumulative AE count, and cumulative AE event curves (see Fig. 4(f–k)), choosing the first significant increase in the gradient of the cumulative curves, again completely depends on the scale of the plot (the upper limit of the right vertical axis that corresponds to the cumulative curves). For example, in the real scale plot, the corresponding displacements to the first significant increase in the gradient of the cumulative AE energy, AE counts, and AE events curves are 7.9, 7.7 and 6.9 mm, while, in the magnified plot, they are 4.7, 4.6 and 5.5 mm, respectively. Therefore, the obtained results from the cumulative curves also depend on the plot scale. The sentry function curve of the DCB specimen is shown in Fig. 4(l). There are two significant drops at the early stage and both drops could be considered as the first "significant" drop. Therefore, one person might choose drop number 1 as the first drop and another person might select drop number 2 as the moment of the damage initiation because of its severity in comparison to the first drop.

In order to avoid the different interpretations of the aforementioned qualitative criteria for damage initiation detection using AE, a quantitative criterion based on the Felicity effect has been proposed in ASTM E2478-11 standard [49], "Determining damage-based design stress for glass fiber reinforced plastic (GFRP) materials using acoustic emission". Accordingly, the damage initiation is specified by the presence of a "significant AE activity" during the reloading portion of the loading/-reloading cycles. The term of "significant AE activity" is determined using a quantitative historic index. In order to obtain the historic index, first, the ultimate strength of the specimen should be determined using a monotonic loading up to the final fracture of the specimen. Then, the similar specimen is subjected to some load/reload cycles. The first load level should be equal to 15% of the ultimate load and it is increased 5% in each subsequent reload cycle. During the reload cycles, the AE signals are recorded until the maximum load of the previous cycle. The historic index is defined as follows [49]:

$$H(t) = \frac{N}{N-K} \frac{\sum_{i=K=1}^{i=N} S_{Oi}}{\sum_{i=1}^{i=N} S_{Oi}} \tag{2}$$

where $H(t)$ is the historic index at time t, N is the number of AE hits up to time t, S_{Oi} is the MARSE value of ith hit (other parameters such as signal strength or energy can also be used) and K is a parameter that is depended to the number of hits and it is obtained from Table 2. The damage initiation is indicated when the historic index becomes equal or greater than 1.4 for the first time.

The last challenge that affects the reliability and reproducibility of AE results for the damage evaluation in laminated composites is the fact that most of the AE descriptors such as amplitude, duration, rise time, central frequency, peak frequency and energy are affected by the source/sensor distance, sensor type, coupling quality, damage accumulation and specimen's geometry (wave mode conversion, dispersion and reflection). For example, Hamstad et al. [50] investigated the propagation of the AE waves during the impact tests of a GFRP pressure vessel. The obtained results showed that some features such as the duration, rise time, amplitude and the spectral content of the signals, originated from the same source, are significantly affected by the source/sensor distance. In addition, the damage state of the structure can affect the AE signals [51]. As the damage accumulates, the medium alters and the recorded AE waveforms, originated from the same damage mechanism but at different damage state of the structure, may have different AE features.

Furthermore, the AE features are also depended on user's input such as the threshold level, the peak definition time (PDT) and hit definition time (HDT) parameters. To overcome this limit the user's influence, Chai et al. [52], proposed a new AE parameter, Shannon's entropy, which is directly extracted from the waveform and its trend is almost similar to counts and energy parameters. The Shannon's entropy represents the uncertainty of the probability amplitude distribution of the AE waveform. An increase in the Shannon's entropy indicates the occurrence of an internal change in the material, which can be due to the damage occurrence. The Shannon's entropy of the AE waveform is obtained in three steps: 1) the voltage per the microsecond values of the waveform should be extracted, 2) the histogram of the discrete probability distribution of the voltage values is plotted with a small bin width, and 3) the Shannon's entropy of each waveform is calculated using Eq. (3) [52]:

$$H = \sum_{i=1}^{n} p(x_i) \cdot \log_2\left(p(x_i)\right) \tag{3}$$

where H is the Shannon's entropy, the waveform's voltage values are given by $\{x_1, x_2, \ldots, x_n\}$ and $p(x_i)$ is the probability mass associated with x_i. The Shannon's entropy is a non-negative value and sum of the probabilities should be equal to 1.

3.2. Identification of different damage mechanisms

A composite structure might experience different types of damage in operation, including but not limited to matrix cracking, fiber breakage, fiber/matrix debonding, delamination and fiber pull-out. As already mentioned, the type of damage depends on several factors, such as the loading direction, loading rate, resin and fiber materials, laminate's

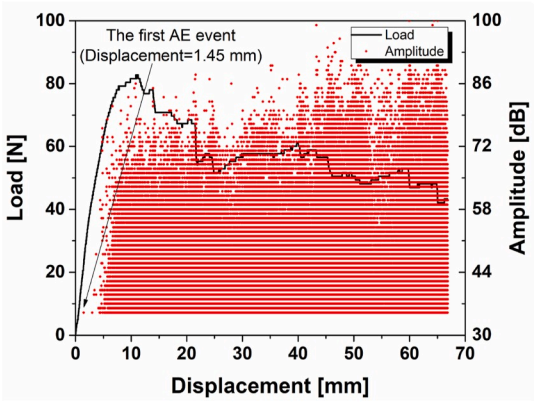

(a) The first detected AE event

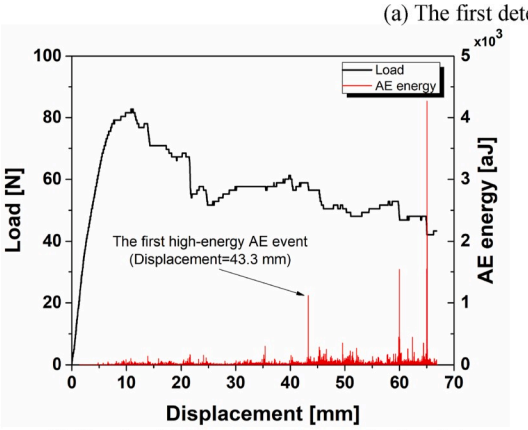

(b) The first high-energy AE event (real scale)

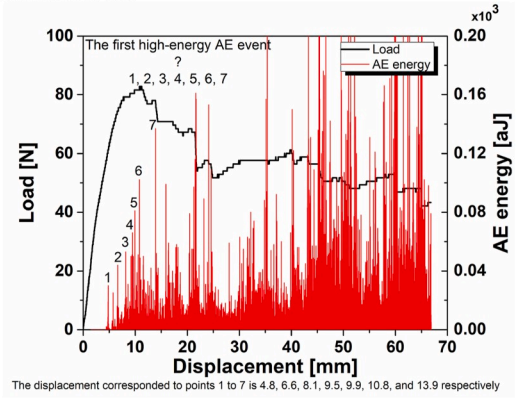

(c) The first high energy-AE event (magnified scale)

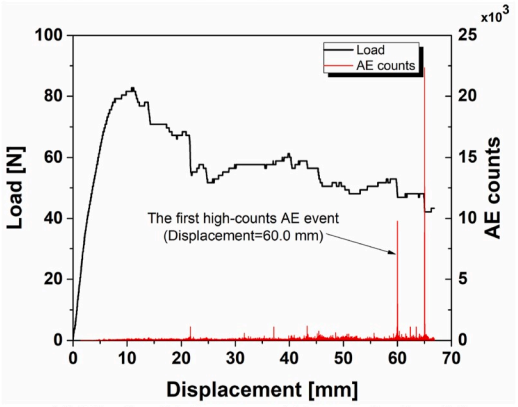

(d) The first high-counts AE event (real scale)

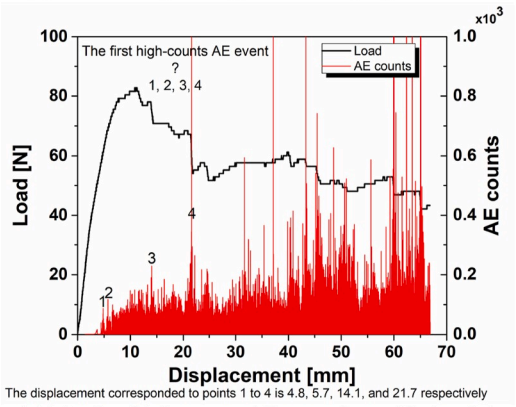

(e) The first high-counts AE event (magnified scale)

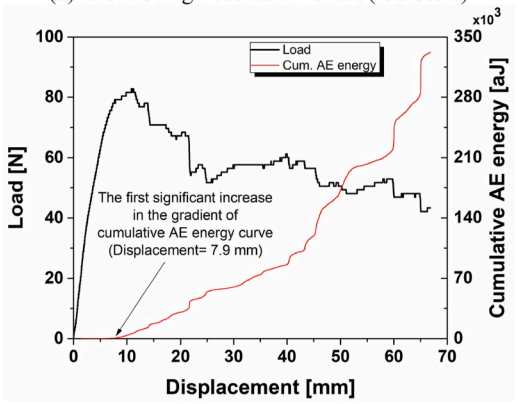

(f) The first significant increase in the gradient of cumulative energy curve (real scale)

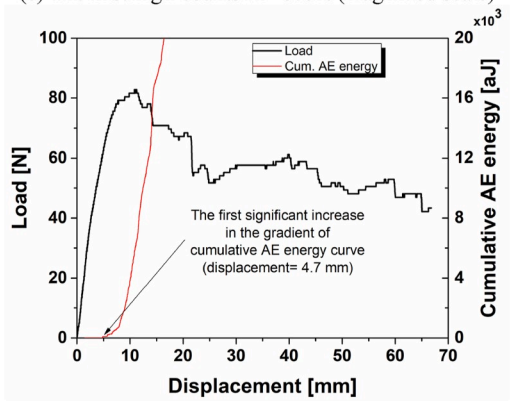

(g) The first significant increase in the gradient of cumulative energy curve (magnified scale)

Fig. 4. Damage initiation detection in glass/epoxy DCB specimen using different AE-based approaches.

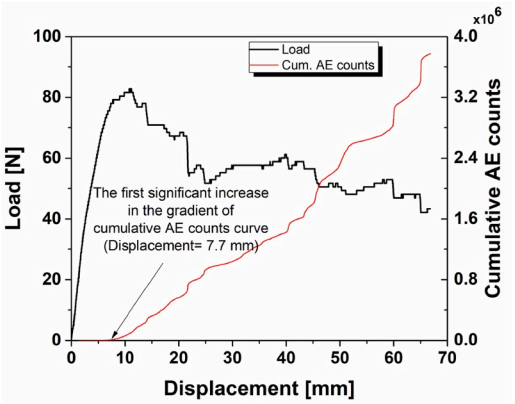

(h) The first significant increase in the gradient of cumulative counts curve (real scale)

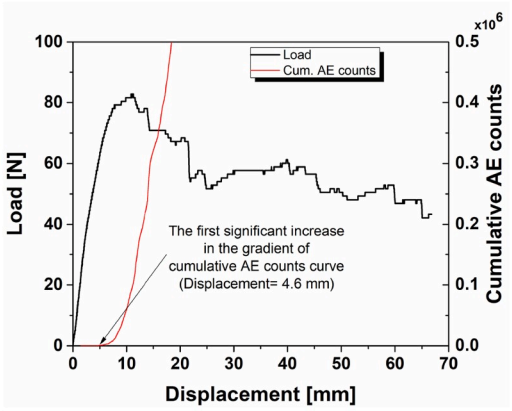

(i) The first significant increase in the gradient of cumulative counts curve (magnified scale)

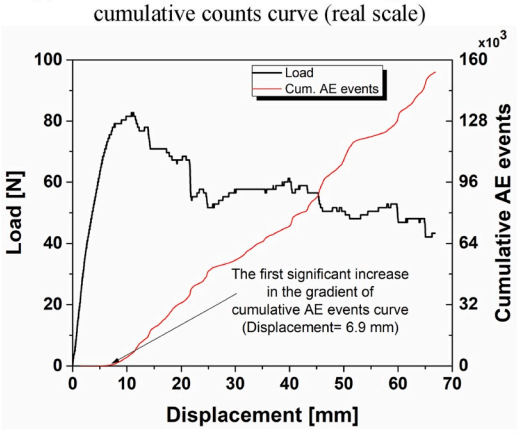

(j) The first significant increase in the gradient of cumulative events curve (real scale)

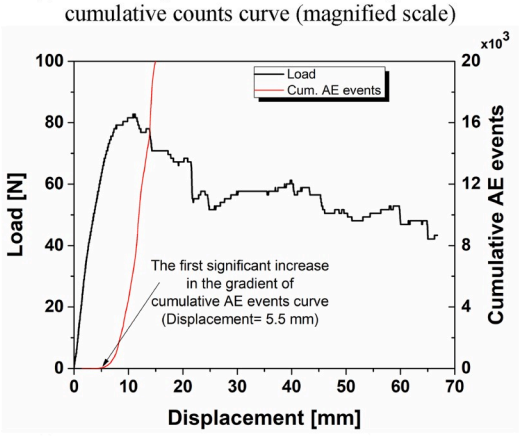

(k) The first significant increase in the gradient of cumulative events curve (magnified scale)

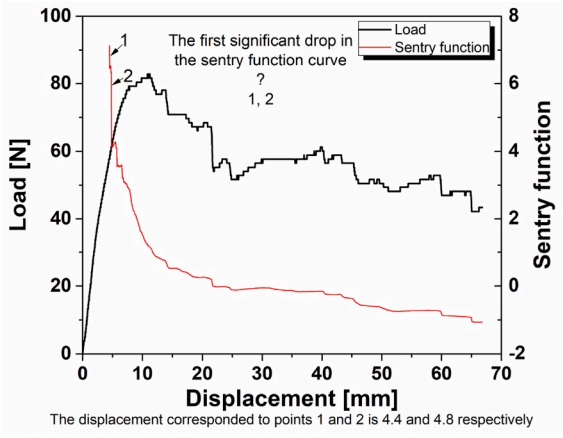

(l) The first significant drop in the sentry function curve

Fig. 4. (*continued*).

Table 2
The values of K parameter for the historic index [49].

K	Number of hits, N
Not applicable	<20
0	20 to 100
0.8 N	101 to 500
N-100	>500

layup, adhesion quality between the fiber and matrix and environmental conditions like temperature and humidity. The impact of these damages on the integrity of the structure is not equal. For example, micro-matrix cracks usually could not drop the stiffness and the integrity of the structure considerably, while delamination and fiber breakage significantly reduce the out-of-plane and in-plane load-bearing capacity of the structure. Therefore, detecting and distinguishing different damage modes can give a better perspective of the integrity state of the structure. In this case, AE technique has shown an excellent capability to identify different damage mechanisms in composite materials. The literature review reveals that each damage mechanism in composite materials usually generates AE signals with almost unique features. For example, matrix cracking is usually characterized by low amplitude, low frequency, long duration, long rise time and large counts. While, delamination is determined by the intermediate amplitude, low frequency and

very long duration. On the other hand, fiber breakage produces signals with high amplitude, high frequency and short rise time [7,64,66,72]. Among all the AE features such as amplitude, rise time, duration, energy, centroid frequency and peak frequency, two features are treated as the most preferred AE features for damage identification: peak frequency and amplitude. Because the peak frequency is not highly affected by the attenuation phenomenon, it seems to be a better damage distinguishing parameter than the amplitude.

Tables 3 and 4 present the reported peak frequency and amplitude in literature for the AE signals of various damage mechanisms in different composites. The variations in the reported values for each damage mode can be related to the different types of sensors, loading conditions, boundary conditions and the sensors' position. Irrespective of the variations, one conclusion is that matrix cracking usually has been identified by the lowest amplitude and frequency while the fiber breakage has been characterized by the highest amplitude and frequency. The delamination and interfacial debonding have been also identified by the average frequency and amplitude. However, Oz et al. [73] showed that this conclusion is not always true. They used in-situ digital image correlation (DIC) and AE to identify different damage modes in CFRP composites subjected to tensile loading. They correlated the recorded AE signals to the DIC results and found that the matrix cracking might also produce some high-frequency signals. They also reported that the amplitude of fiber breakage signals depends on the relative position of the damage respect to the specimen's boundary. Thus, it is highly recommended that other complementary in-situ techniques like DIC, camera, and thermography are employed during the tests to find the sources of the originated AE signals. The results obtained from these techniques can be used in parallel to AE results to correlate the clusters of AE signals to the corresponded damage mechanisms confidently.

Distinguishing the AE signals originated from different damage mechanisms is still a challenging issue. This is because in a real composite structure, subjected to an arbitrary load, several damages usually occur simultaneously and their AE signals arrive at the sensor at the same time. Therefore, correlating each signal to a specific damage mode is not straightforward.

One solution for this problem is designing the specific test coupons with the biased damage modes, in a way that just one damage mode occurs in the coupon or at least one damage mode be the dominant one. Accordingly, the AE features of that damage mode could be captured irrespective of the other damages. By changing the coupon design, layup and loading condition, the AE signals of other damages can also be collected with the minimum interference together. For example, de Groot et al. [74] distinguished the different damage mechanisms, including matrix cracking, fiber/matrix debonding, fiber pullout and fiber breakage in carbon/epoxy laminates based on their frequency. To this aim, they designed and performed a couple of tests, including the tensile test on pure resin, uncured prepregs, 0°, 10° and 90° coupons, and the fracture tests on the DCB and single lap joint specimens. The results showed that the AE signals of the pure resin and 90° coupons tensile tests are only generated by matrix cracking. While, in the case of DCB and single lap shear specimens, in addition to the matrix cracking, debonding also happened in the specimens. In the case of the tensile test of 0° coupons, besides the two previous damage modes, the fiber breakage and fiber pull-out were also observed. All the damage modes observed in 0° coupons occurred in 10° coupons again, except the fiber breakage. Finally, they could identify and distinguish the AE signals of all aforementioned damage modes by comparing the AE frequency of these tests (see Table 5).

Gutkin et al. [75] conducted five different types of test, including

Table 3
The AE peak frequency (in kHz unit) of different damage mechanisms reported in the literature.

Reference	Material	Type of the test	Matrix cracking	Fiber/matrix debonding	Delamination	Fiber breakage	Fiber pullout
CFRP							
[74]	Carbon/epoxy	Tensile	90–180	240–310	–	>300	180–240
[75]	Carbon/epoxy	Tensile, compact tension, compact compression, DCB and 4-ENF	<50	200–300	50–150	400–500	500–600
[99]	Carbon/epoxy	Tensile	<300	–	–	>500	>500
[5]	Carbon/epoxy	Quasi-static indentation	<150	–	150–300	>400	–
[100]	Carbon/epoxy	3 PB	60–120	–	120–210	200–350	–
[38]	Carbon/epoxy	Tensile	–	–	250–330	>450	–
[101]	Carbon/epoxy	Tensile	<100	200–300	–	400–450	–
[102]	Carbon/epoxy	Tensile	20–400	30–400	120–360	50–500	–
[103]	Graphite/epoxy	Tensile	<120	–	–	120–180	–
[104]	2D woven carbon/epoxy	Tensile	<100	150–300	<100	350–600	
[105]	2D and 3D woven carbon/epoxy	Tensile	<300	–	–	>300	–
GFRP							
[63]	Glass/epoxy	DCB	140–250	250–350	–	350–450	–
[77]	Glass/epoxy	Open-hole tensile (OHT)	80–250	250–375	–	375–480	–
[106]	Glass/polypropylene	Tensile	–	Around 100	–	450–550	200–300
[107]	GFRP	45.7-m long wind turbine blade loaded in the flap-wise direction	<30	120–250	30–120	–	–
[108]	2D woven glass/epoxy	Tensile	<180	–	>180	>180	–
[109]	2D and 3D woven glass/epoxy	Tensile	50–80	50–150	150–500	150–500	–
Other types of composites							
[72]	Kevlar-woven composites	High strain rate impact	Near 106	Near 110	–	>300	Near 110
Hybrid							
[110]	Hybrid of carbon & glass/epoxy	Tensile	200–600	200–350	100–500	>1500	700–1100
[54]	Sandwich composite with glass/epoxy skins	DCB	170–250	–	50–170	350–500	–
[111]	carbon/Kevlar hybrid woven composites	High strain rate compressive loading	Near 190	Near 110	–	(Near 400 for carbon) (Near 350 for Kevlar)	Near 110
[112]	Glare, graphite/epoxy and carbon/carbon	Tensile, compact tension, Flexural	Around 140	Around 300	–	Around 405	–

Table 4
The AE amplitude (in dB unit) of different damage mechanisms reported in the literature.

Reference	Material	Type of the test	Matrix cracking	Fiber/matrix debonding	delamination	Fiber breakage	Fiber pullout
CFRP							
[113]	Carbon/epoxy	Tensile fatigue	60–77	–	77–90	–	>90
[114]	Carbon/epoxy	OHT	40–60	50–70	60–80	80–100	80–100
[102]	Carbon/epoxy	Tensile	60–100	45–65	60–95	<60	–
[85]	Carbon/epoxy	Tensile	Around 60	–	Around 80	Around 80	–
[115]	Carbon/epoxy	Tensile	40–70	–	–	60–100	–
[99]	Carbon/epoxy	Tensile	<70	–	<60	–	–
[38]	Carbon/epoxy	Tensile	–	–	>90	40–60	–
[116]	Carbon/epoxy	3 PB	Around 50	–	Around 62	–	–
[105]	2D and 3D woven carbon/epoxy	Tensile	<70	–	–	30–90	–
GFRP							
[117]	Glass/epoxy	Tensile	40–80	50–80	70–100	70–100	70–100
[69]	Glass/epoxy	DCB	–	–	–	85–100	–
[118]	Glass/epoxy	Torque loading	33–45	50–68	–	87–100	69–86
[119]	Glass/epoxy	Tensile and flexural tests	60–80	–	70–90	–	–
[120]	Glass/polyester	Fatigue bending	40–55	–	55–75	>80	–
[121]	Glass/polypropylene	Tensile, tensile fatigue and crack propagation tests	40–55	60–65	60–65	85–95	65–85
[108]	2D woven glass/epoxy	Tensile	<55	–	>55	35–100	–
[109]	2D and 3D glass/epoxy	Tensile	35–55	55–100	35–80	35–80	–
Other types of composites							
[72]	Kevlar-woven composites	High strain rate impact	42–48	50–65	–	>70	50–65
[122]	UHMWPE/HDPE	Tensile	30–60	30–45	60–85	80–97	60–80
Hybrid							
[54]	Sandwich composite with glass/epoxy skins	DCB	75–85	–	60–80	85–105	–
[111]	Carbon/Kevlar hybrid woven composites	high strain rate compressive loading	42–43	50–67	–	(94–99 for carbon) (70–87 for Kevlar)	50–67
[123]	Sandwich composites with CFRP skin	Tensile	80–90	–	–	>90	–
[124]	Sandwich composite with glass/epoxy skins	3 PB	40–78	–	72–100	95–100	–

tensile, compact tension, compact compression, DCB and ENF, on CFRP coupons to obtain the AE frequency of the five different damage mechanisms. These damages were matrix cracking, fiber breakage, fiber/matrix debonding, delamination and fiber pull-out. Saeedifar et al. [76] distinguished the AE signals of different damage mechanisms in the adhesively-bonded hybrid double-lap joints using AE. The damages observed in the double lap joints were CFRP skin failure, core steel deformation, adhesive layer failure (which was named cohesive failure) and debonding at the interface of the adhesive layer with CFRP skin or steel core (which was name adhesive failure). In order to characterize the AE signals of these damages, they conducted four series of tests on the constituent materials: 1) the tensile and shear tests of steel, 2) tensile, in-plane mode I and mode II shear tests of adhesive, 3) tensile test of CFRP and 4) DCB test of CFRP to CFRP and steel to steel adhesively-bonded coupons. To obtain the AE signals of matrix cracking and fiber breakage, some researchers [54,77] performed tensile tests on pure resin and fiber bundle coupons while the originated AE signals were recorded. This damage identification process requires a large experimental effort and a database with AE characteristics of each individual damage mechanism should be created. As aforementioned, the AE features of each damage mechanism could be obtained by performing the individual constituent tests, but the AE dataset of a damaged composite structure usually contains the AE signals of several damage mechanisms mixed together.

The second level of damage assessment of a composite structure is partitioning the AE signals of different damage mechanisms. This process is usually done according to one of the four following ways: 1) manual discriminating of the AE data, 2) unsupervised clustering, 3) supervised classification and 4) signals processing. The details of the studies devoted to the damage identification and damage clustering using AE are presented in Table 5. Some literature [44,64,74] used one or two AE features, mostly peak frequency and amplitude, to manually group the AE data and to correlate them to the different damage modes. For instance, Nikhbakht et al. [44] manually categorized the AE data recorded during the DCB test into three groups based on their frequency. They correlated these groups to matrix cracking, fiber/matrix debonding and fiber breakage. They also used the in-situ microscopy images to verify the AE results. However, sometimes different damage mechanisms are not completely differentiated using just one AE feature. In this situation, it is better to use multiple AE features simultaneously to identify the damage type with more confidence. In this case, due to the complex relations among the different AE features, the data partitioning process is usually done by the machine learning techniques: unsupervised and supervised techniques. Unsupervised clustering techniques like k-means, genetic k-means (GKM), fuzzy c-means (FCM), Gaussian mixture distribution (GMD), self-organizing map (SOM) and hierarchical models have been frequently used for damage clustering in composite materials. Generally, all unsupervised clustering techniques try to partition a set of AE signals, $\{X_1, X_2, \ldots, X_n\}$, each signal has been defined by p features, $X_1 = [x_1, x_2, \ldots, x_p]$), into k clusters ($k \leq n$), $\{C_1, C_2, \ldots, C_k\}$. Among the unsupervised clustering techniques, k-means has been widely used in literature to discriminate different damage mechanisms in laminated composites [4,78–82]. K-means clusters AE data in two steps; it first selects the initial clusters' centroid randomly and each data point is assigned to the cluster with the nearest cluster's centroid (Eq. (4)). In the second step, the new centroid of each cluster is updated to the average value of all the data points, which are inside the cluster (Eq. (5)) [83]:

$$C_i^{(t)} = \left\{ X_n : \left\| X_n - m_i^{(t)} \right\|^2 \leq \left\| X_n - m_j^{(t)} \right\|^2 \forall j, 1 \leq j \leq k \right\} \tag{4}$$

$$m_i^{(t+1)} = \frac{1}{\left| C_i^{(t)} \right|} \sum_{X_j \in C_i^{(t)}} X_j \tag{5}$$

Table 5
Damage distinguishing in laminated composites using AE.

Material	Type of the test	Types of damage	Utilized method	Utilized AE parameters	The utilized method to validate AE results	Ref.
The manual partitioning of AE data						
Carbon/epoxy	Tensile	Matrix cracking, fiber/matrix debonding, fiber pullout and fiber breakage	Manual clustering	Peak frequency	Performing the tensile tests on resin, uncured prepregs, 0° and 90° coupons, and also DCB specimens.	[74]
Hybrid of thin carbon/epoxy and conventional glass/epoxy	Tensile	Fiber fracture and ply fragmentation	Manual clustering	Amplitude and AE energy	Visual inspection of the specimens	[64]
Glass/epoxy	DCB	Matrix cracking, fiber/matrix debonding and fiber breakage	Manual clustering	Peak frequency	Microscopy images	[44]
Glass/epoxy	Tensile and compression tests on dogbone samples and single-lap bonded joints	Matrix micro crack, matrix macro crack and fiber breakage	Manual clustering	Peak frequency	DIC	[125]
Damage partitioning using one method Unsupervised and supervised techniques						
Glass/epoxy	Quasi-static and fatigue tensile tests	Matrix cracking, fiber/matrix debonding, delamination, fiber breakage	k-means	Amplitude, energy, rise time, counts and duration	SEM images from the fractured surfaces	[4]
Carbon/flax fiber hybrid composites	Tensile	Matrix cracking, fiber/matrix debonding, delamination and fiber breakage	k-means	Amplitude, absolute energy, duration, counts to peak and rise-time	SEM images from the fractured surfaces	[79]
Glass/carbon fiber hybrid composites	Pure bending and tensile tests	Matrix cracking, interface failure, fiber breakage and fiber pull out	k-means	Amplitude, Counts, Rise time, Peak frequency, weighted frequency, partial powers	Weighted peak frequency and partial power	[82]
Woven carbon/epoxy	Tensile and flexural tests	Matrix cracking, interface failure and fiber breakage	k-means	Weighted peak frequency and partial power 1	SEM and DIC	[78]
Flax, glass and hybrid flax-glass fiber woven composites	DCB	Matrix cracking, interface failure, delamination and fiber breakage	k-means	amplitude, duration, number of counts, energy and rise time	SEM	[81]
Flax fiber reinforced thermoplastic composite	Quasi-static and fatigue tensile tests	Matrix micro-cracking, fiber-matrix debonding, fiber pull-out and fiber breakage	k-means	Amplitude, duration, rise time, energy and numbers of counts to peak	–	[80]
2D and 3D woven carbon fiber/epoxy	Tensile	Matrix cracking, delamination and fiber breakage	k-means++	Amplitude, peak frequency and centroid frequency	–	[105]
Glass/epoxy	3 PB	Matrix cracking, fiber/matrix debonding and fiber breakage	FCM	Amplitude, duration and average frequency	SEM images	[7]
Glass/epoxy and carbon/epoxy	Tensile test on rod type specimens	Matrix cracking, fiber/matrix debonding and fiber breakage	FCM	Duration, peak amplitude, energy, and the number of counts	SEM images	[36]
Hemp/epoxy and Glass/epoxy	3 PB	Matrix cracking, delamination, Interfacial debonding and fiber breakage	GMD	Peak frequency	–	[66]
Glass/epoxy	Buckling	Matrix cracking, delamination and fiber breakage	GMD	Peak frequency and amplitude	Camera images	[71]
Carbon/epoxy	Tensile	Matrix cracking, delamination and fiber breakage	SVM	Rise time, counts, duration, amplitude and energy	–	[85]
Carbon/carbon	Tensile	Matrix cracking, fiber/matrix debonding, fiber pullout, thermal stress relief, fiber arrangement to the loading direction, matrix friction, fiber push-in and single fibers and fiber bundles failure	Unsupervised clustering	Parametric load, amplitude, rise angle, reverberation frequency	–	[126]
Hybrid of flax/epoxy and glass/epoxy	Tensile	Matrix cracking, fiber breakage and fiber/matrix debonding	Combining principal component analysis (PCA) and FCM	Amplitude, duration, rise time, counts and energy	SEM images	[86]
Glass/epoxy	Creep tensile	Matrix cracking, fiber breakage and fiber/matrix debonding	Combining PCA and FCM	Duration, sum and maximum of the square moduli of continues wavelet transform coefficients and maximum of the square discrete wavelet transform detail coefficients	–	[87]
Sandwich composite with glass/epoxy skin and foam core	DCB	Interfacial debonding, matrix cracking, fiber breakage and core failure	Combining PCA and GKM	Amplitude, peak frequency and energy	Camera and SEM images	[61]

(*continued on next page*)

Table 5 (*continued*)

Glass/polyester	DCB	Matrix cracking, fiber/matrix debonding and fiber breakage	Combining PCA and FCM	Energy, amplitude, rise time, counts, peak frequency and duration	–	[88]
Adhesively-bonded hybrid double lap joint	Tensile	Steel core failure, adhesive failure, cohesive failure and CFRP skin failure	Ensemble bagged trees	Amplitude, rise time, duration, counts, energy, RMS, centroid frequency and peak frequency	DIC and fiber optic sensor	[76]
Signal processing methods						
Glass/epoxy	3 PB	Matrix cracking, fiber breakage and fiber/matrix debonding	WT	The AE waveform	SEM images	[53]
Carbon/epoxy	Tensile	Matrix cracking, fiber/matrix debonding, fiber pull-out and fiber breakage	WT	The AE waveform	SEM images	[95]
Sandwich composite with glass/epoxy skin and foam core	DCB	Core failure, adhesive bond failure, matrix cracking and fiber breakage	WT	The AE waveform	Camera and SEM images	[54]
Glass/epoxy	Tensile test of the drilled specimen	Matrix cracking, fiber slippage and fiber breakage	WT	The AE waveform	SEM images	[59]
Glass/polyester	OHT	Fiber failure	WT	The AE waveform	–	[127]
Glass/epoxy	ENF	Matrix cracking, fiber/matrix debonding and fiber breakage	HT	The AE waveform	SEM images	[60]
Damage partitioning using multiple methods						
Glass/epoxy	DCB, ENF and MMB	Matrix cracking, fiber/matrix debonding and fiber breakage	Combining PCA and FCM, packet wavelet transform	Amplitude, frequency, energy, count, rise time, and duration	SEM images	[41]
Glass/epoxy	3 PB	Matrix cracking, fiber breakage and fiber/matrix debonding	Combining PCA and FCM, packet wavelet transform	The AE waveform and three parameters, including peak amplitude, average frequency and counts	SEM images	[40]
Glass/epoxy	Quasi-static indentation	Matrix cracking, fiber/matrix debonding and fiber breakage	Combining PCA and FCM, packet wavelet transform	The AE waveform and five AE parameters, including amplitude, duration, rise time, counting, and average frequency	–	[55]
Glass/epoxy	3 PB	Matrix cracking, fiber/matrix debonding, fiber breakage and delamination	Hilbert-Huang transform and k-means	The AE waveform, duration, peak amplitude, counts, rise time and energy	–	[128]
Carbon/epoxy	Buckling	Matrix cracking and delamination	Combining PCA and k-means, FCM	17 parameters, including rise time, decay time, counts, duration, energy, amplitude, average frequency, absolute energy, etc.	–	[129]
Carbon/epoxy	OHT, 4 PB and tensile tests	Crack growth and fiber failure	k-means, FCM, hierarchical model and GMD	Amplitude and peak frequency	DIC	[92]
Carbon/epoxy	Quasi-static indentation	Matrix cracking, delamination and fiber breakage	k-means, GKM, FCM, SOM, GMD and hierarchical model	Amplitude and peak frequency	Microscopy and C-scan images	[5]

where $C_i^{(t)}$ is cluster i and $m_i^{(t)}$ is the center of cluster i at iteration t.

These two steps are repeated until the stop criterion is met, i.e. the maximum number of iterations or a minimum value of changing the cluster centroid's position between two consequent iterations. Although this technique is simple and has a low computational cost, there is no guarantee that it always converges to the optimum results. In other words, there is a possibility that the algorithm partitions data incorrectly. This is due to the random selection of the initial clusters' centroids (refer to Ref. [83] to find more details about this method). To overcome this limitation, some researchers tried to improve this technique by adding a fuzziness parameter to k-means, which is named fuzzy c-means (FCM), or combining k-means with the genetic algorithm, which is named genetic k-means (GKM) algorithm. The clustering process using FCM is similar to k-means with the difference that in FCM, a membership parameter is defined that allows a data point belongs to more than one cluster at the same time, with different membership values from 0 to 1 (more details about this technique can be found in Ref. [84]). To find the best clustering, FCM tries to minimize objective function $J(X;C)$ (Eq. (6)) [84]:

$$J(X;C) = \sum_{i=1}^{k}\sum_{j=1}^{n} (\gamma_{ij})^{\alpha} \|X_j - C_i\|^2 \tag{6}$$

$$D_{ij}^2 = \|X_j - C_i\|^2 = (X_j - C_i)^T (X_j - C_i)$$

where γ_{ij} is the membership parameter and α is the fuzzier. The objective function will be minimized if [84]:

$$\gamma_{ij} = \frac{1}{\sum_{m=1}^{k} \left(\frac{D_{ij}}{D_{mj}}\right)^{\frac{2}{\alpha-1}}}; 1 \le i \le k, 1 \le j \le n \tag{7}$$

and

$$C_i = \frac{\sum_{j=1}^{n} (\gamma_{ij})^{\alpha} X_j}{\sum_{j=1}^{n} (\gamma_{ij})^{\alpha}}; \quad 1 \le i \le k \tag{8}$$

In the case of GKM algorithm, the genetic algorithm is used to create better clusters' centroids in the new iterations by crossover of the previous clusters' centroids (more details about this technique can be found in Ref. [61]). FCM and GKM have been widely used for damage clustering in composite materials under different loading conditions such as tensile [36,85,86], creep tensile [87], 3 PB [7] and fracture mode I [61,88]. Besides k-means-based methods, other methods like GMD and SOM have been also utilized for damage clustering in composites [5,66,71].

GMD assumes that the whole dataset can be expressed as a weighted summation of several Gaussian densities with unknown parameters ($p(x)$) [89]:

$$p(x) = \sum_{k=1}^{K} w_k g\left(X \middle| \mu_k, \sum_k\right) \tag{9}$$

$$g\left(X \middle| \mu_k, \sum_k\right) = \frac{1}{\sqrt{(2\pi)^k \left|\sum_k\right|}} \exp\left(\frac{-\frac{1}{2}(X-\mu_k)^T}{\sum_k (X-\mu_k)}\right)$$

$$\sum_{k=1}^{K} w_k = 1$$

where g is the Gaussian density function with mean vector μ_k and covariance matrix Σ_k, X is data and w_k is the mixture weight function.

First, the algorithm estimates random initial values for mean vectors and covariance matrices of density distributions. Then, it calculates weight function values for all the data points and the mixture distributions. Afterward, the new mean vectors and covariance matrices are updated (Eqs. (10)and (11)). This process is repeated until the stop criterion is satisfied which can be the maximum number of iterations (more details can be found in Ref. [89]).

$$\mu_k^{new} = \left(\frac{1}{N_k}\right) \sum_{i=1}^{n} w_{ik} \cdot X_i; \quad 1 \le k \le K \tag{10}$$

$$\sum_k^{new} = \left(\frac{1}{N_k}\right) \sum_{i=1}^{n} w_{ik} \cdot \left(X_i - \mu_k^{new}\right)\left(X_i - \mu_k^{new}\right)^T; \quad 1 \le k \le K \tag{11}$$

$$w_k^{new} = \frac{N_k}{N}; \quad 1 \le k \le K$$

where N_K is sum of membership weight for kth component defined as $N_K = \Sigma w_{ik}$.

The SOM is a type of artificial neural network (ANN) that can be used in data clustering. The SOM is constructed of a number of weighted neurons in a lattice structure. When a new data point comes into the lattice, the neuron that has the most similarity to the new data owns it. Then, the weight functions (W) of the winner neuron and the neighbor neurons are updated as follows [90]:

$$W_v(t+1) = W_v(s) + \theta(u, v, t) \cdot (X_i - W_v(t)) \tag{12}$$

$$\theta(u, v, t) = \exp\left(\frac{\|r_u - r_v\|^2}{2\sigma^2(t)}\right) \tag{13}$$

where u is the label of the winning neuron for data point X, $\theta(u, v, t)$ is the neighborhood function which expresses the distance between neuron u and v, t is the time step. The positions of neurons u and v are represented by r_u and r_v, and finally $\sigma(t)$ is the neighborhood function's width. By feeding new data to the algorithm, the shape of the lattice gradually changes to get into the shape of the dataset. Finally, according to the new positions of the lattice neurons, the dataset is clustered (more information can be found in Ref. [90]).

Data clustering by the hierarchical model is simple and it is performed in one of the two forms: divisive and agglomerative. In the divisive procedure, each data point is initially considered as a cluster. Then, the algorithm finds two nearest clusters and create a new cluster containing both data points. The algorithm calculates the distance among the new cluster and the old ones again and merges the two closest clusters. This process is continued to reach the desired number of clusters. The agglomerative procedure is exactly the reverse of the divisive. The drawback of the hierarchical model is the low rate of the clustering process (more information can be obtained in Ref. [91]). Although all the aforementioned techniques have been used frequently in literature, nobody reported the limitations of these techniques for the clustering of AE signals. Saeedifar et al. [5] compared the performance of six different unsupervised clustering techniques, including k-means, FCM, GKM, SOM, GMD, and hierarchical for partitioning the AE data of CFRP laminates, subjected to the indentation load. They tried to discriminate three damage mechanisms, including matrix cracking, delamination and fiber breakage with the corresponding frequency ranges of <150 kHz, [150–300 kHz] and >500 kHz, respectively. As depicted in Fig. 5, among the 6 techniques, k-means and GMD failed to cluster the initial AE dataset correctly. To compare the performance of the four other techniques, they created a more complex artificial AE dataset by adding another dense data group to the original AE dataset (a new AE data group with the frequency of less than 50 kHz shown in Fig. 6). As illustrated in Fig. 6, although all the 4 techniques could cluster the new dataset appropriately, the results of FCM, SOM and GKM were not reproducible. In other words, whenever the computer program of these techniques was run, the obtained clusters were changing. The only technique that always gives the same optimum data clustering result was the hierarchical model.

Sawan et al. [92] used four techniques consisting of k-means, hierarchal, FCM, and GMD for AE signals distinguishing in open hole tensile CFRP specimens, subjected to the tensile and bending loading conditions. The results showed that only the GMD model could distinguish AE data appropriately. Thus, it seems that the performance of unsupervised clustering techniques depends on the AE dataset. For example, for a simple AE dataset, which the AE features of different damages have the minimum overlap, a simple technique like k-means might works properly, while in the case of a more complicated AE dataset, a more powerful technique like the hierarchical model should be used. In addition, the repeatability of the clustering results should be checked.

The unsupervised clustering methods have some kinds of intrinsic blindness to partition data and they could not entirely realize the inherent structure of the dataset [76]. In addition, the outputs of these techniques are not labeled, thus it is not known which cluster is related to which damage mechanism. Therefore, if some well-labeled training dataset is available, the use of supervised classification techniques is preferred over the unsupervised techniques. The supervised classification process is generally performed in two steps: 1) the classifier is trained by a training dataset that has been labeled already. 2) After sufficient training of the classifier, it will be used to classify the unknown dataset. Saeedifar et al. [76] used the ensemble decision tree supervised classifier to distinguish four damage mechanisms in the adhesively bonded double lap joint coupons. To obtain the training AE dataset, they conducted several destructive tests on the constituent materials. Then, this dataset was used to train the ensemble model. When the model was sufficiently trained, it was employed to classify damage in the double lap joint coupon. The AE results were validated by the camera images, DIC and fiber optic sensor results.

The last group of researchers used the signal processing techniques for distinguishing damage modes in composite materials. The frequently used technique in this group is wavelet transform (WT). In WT, a signal is decomposed into low and high frequency subcomponents. Based on the type of WT, both of the low and high frequency parts (packet wavelet transform) or just the low frequency part (discrete wavelet transform) will be decomposed in the other levels till the original signal finally is decomposed into several subcomponents with different frequencies (see Fig. 7). Then, based on the frequency of subcomponents, one or some of them are correlated to the specific damage modes. In the case of AE signals, because most of the times valuable information is placed in the high frequency components (for example, fiber damage signals), packet wavelet transform is usually preferred over discrete wavelet transform.

The frequency range of each subcomponent in the packet wavelet transform tree is calculated using Eq. (14) [93]:

$$\left[nf_s 2^{-(i+1)}, (n+1)f_s 2^{-(i+1)}\right] \tag{14}$$

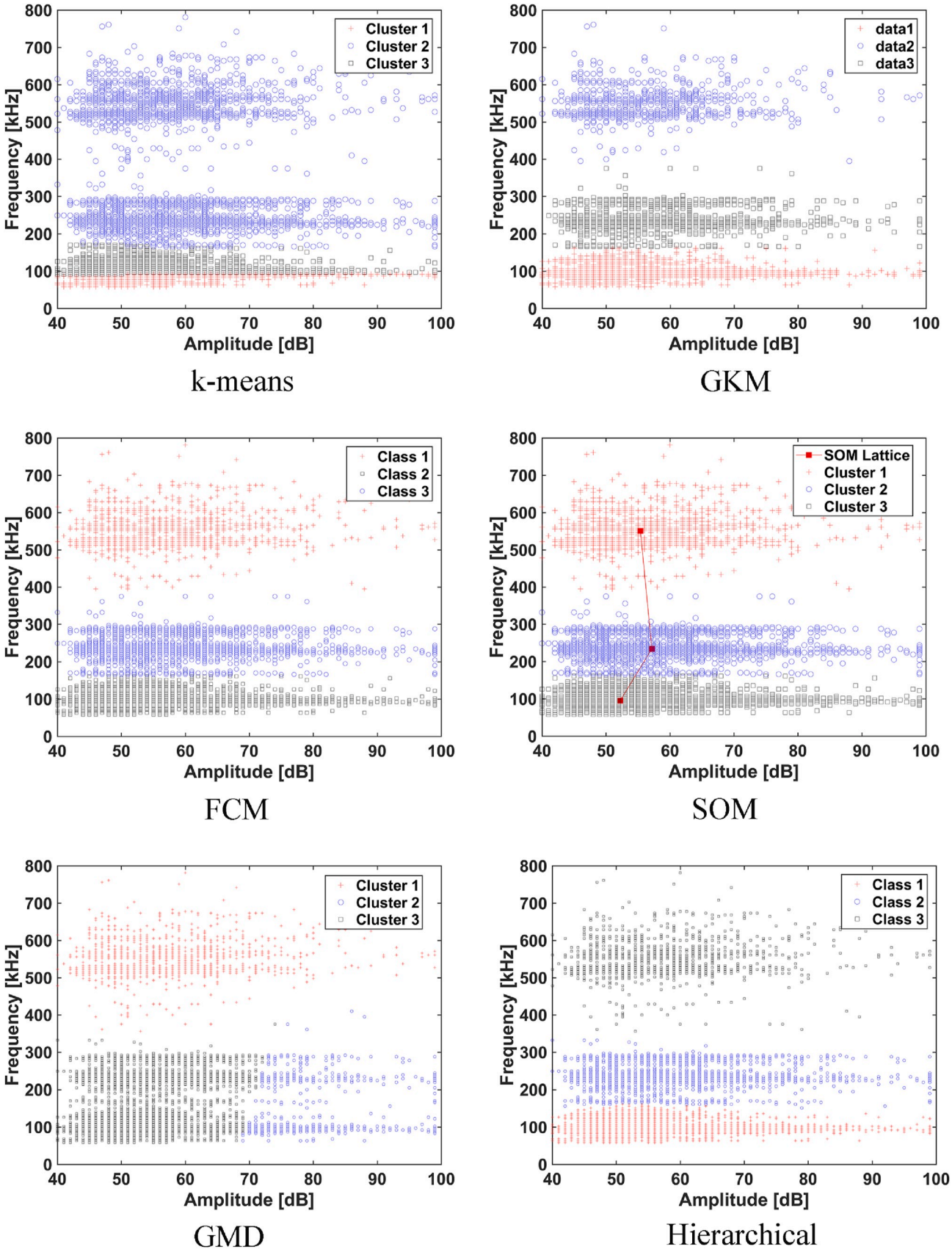

Fig. 5. The performance of k-means, GKM, FCM, SOM, GMD and hierarchical methods to partition the AE signals into three groups (the data belongs to carbon/epoxy laminates subjected to the indentation load) [5].

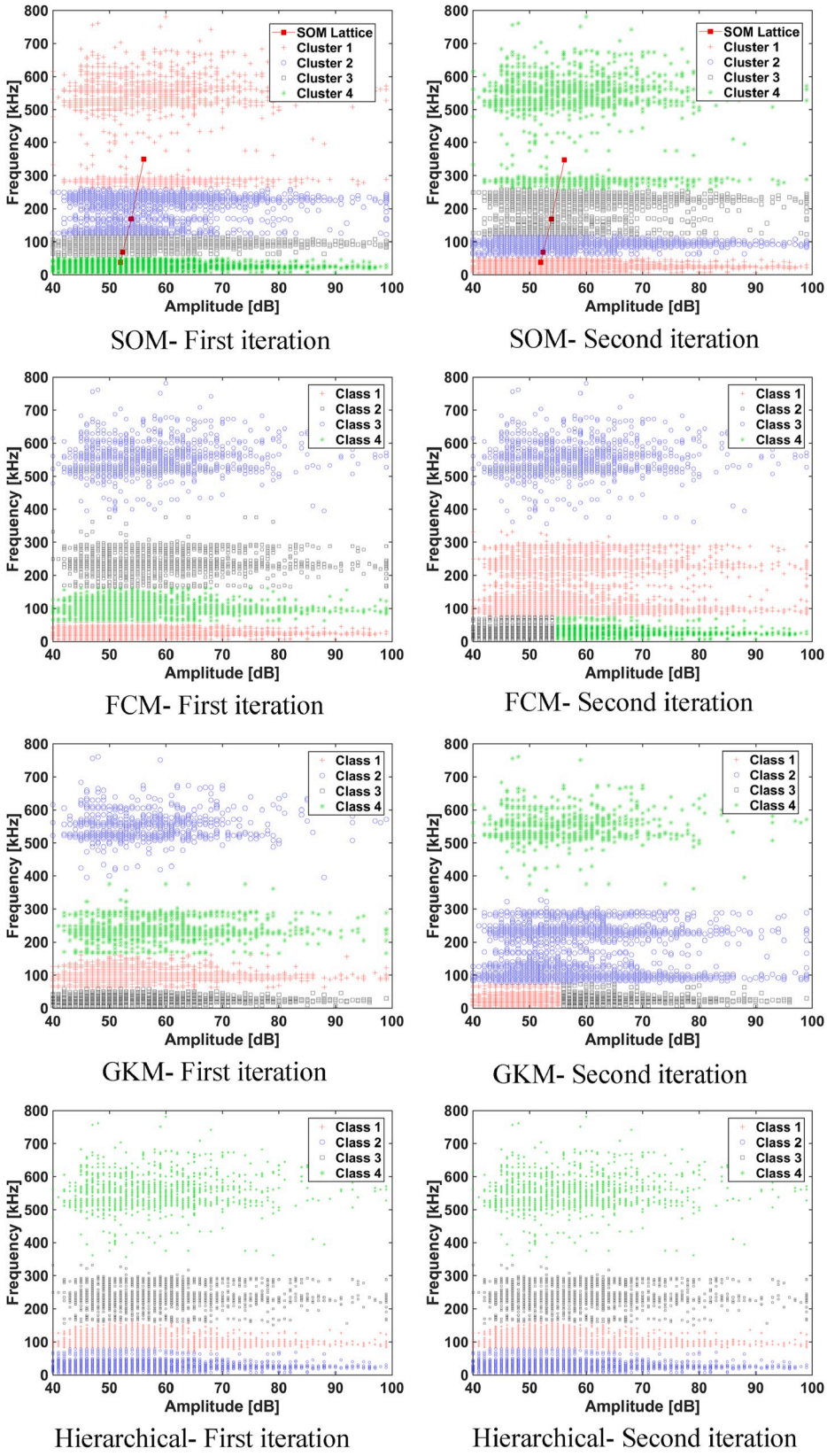

Fig. 6. The performance of SOM, FCM, GKM and hierarchical methods to partition the artificial AE dataset into four groups at different iterations [5].

where f_s is the AE sampling rate, i shows the level of decomposition, and n shows the label of subcomponent, which is equal to $n = 0, 1, \ldots, 2^{i-1}$ for decomposition level i.

The energy percentage of each subcomponent, respect to the original signal, shows the amount of its corresponding damage mode in the composite structure (more information about WT can be found in Refs. [93,94]):

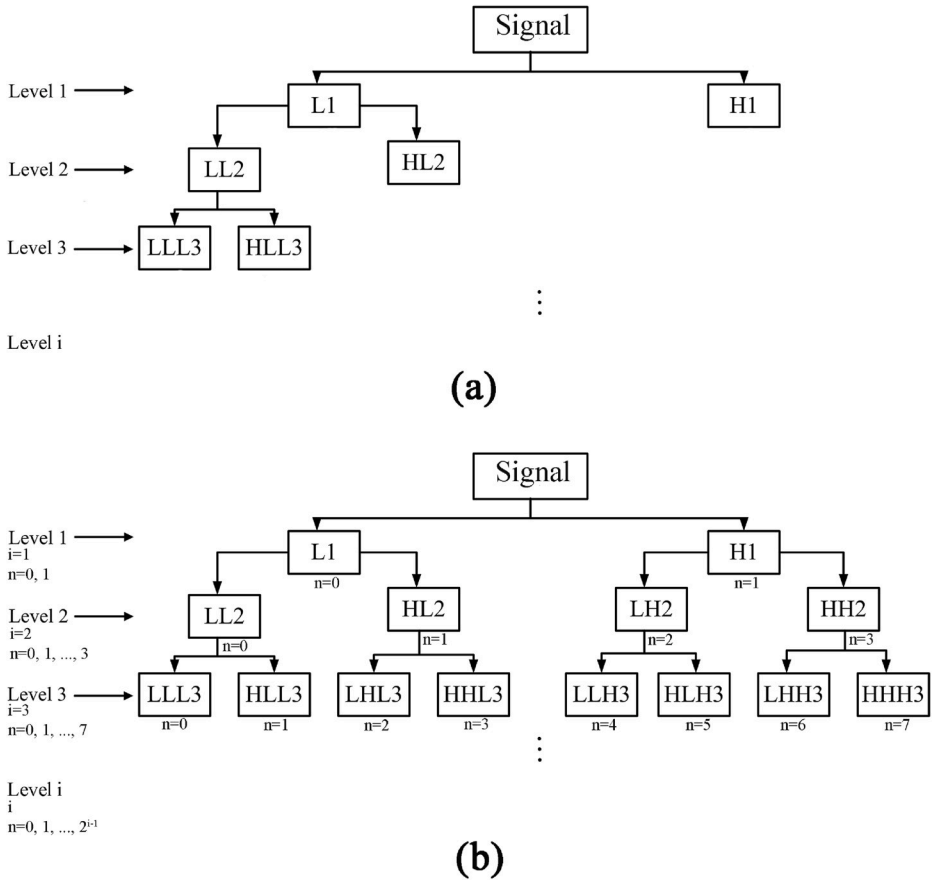

Fig. 7. a) Discrete wavelet transform and b) packet wavelet transform tree (L: low frequency subcomponent and H: high frequency subcomponent).

$$E_i^n = \sum_{T=t_0^n}^{t_1^n} \left[f_i^n(T)\right]^2 \tag{15}$$

$$P_i^n = \frac{E_i^n}{\sum_i \sum_n^{2^{i-1}} E_i^n} \tag{16}$$

where E_i^n is the energy of subcomponent n located in level i, f_i^n is the wavelet subcomponent, t_0^n and t_1^n show its time period, and P_i^n represents the energy percentage of the subcomponent respect to the original signal.

WT technique has been used successfully for damage mechanisms identification in FRP composites subjected to tensile [59,95,96], fracture modes I, II, mixed-mode I&II [40,41,54,60] and LVI [55,97] loading conditions. In addition, a good consistency between the quantified damages by this technique and the other unsupervised techniques like FCM [40,41,55] and hierarchical model [97] has been reported in the literature. Beside WT, some other signal processing techniques have been rarely used in literature. For example, Beheshtizadeh et al. [98] compared the performance of Choi–Williams transform with WT for damage characterization in glass/epoxy and carbon/epoxy laminates, subjected to 3 PB loading conditions. They reported that the sensitivity of WT to the low-intensity part of the signals is higher than Choi–Williams. It is due to the fact that the exponential kernel function of the Choi–Williams transform resulted in the missing of some small details. The last signal processing technique used in literature is Hilbert transform (HT). Nazmdar et al. [60] used HT to determine the damage type in glass/epoxy ENF specimens. They used the phase angle parameter of HT as a feature to obtain the frequency of different damage modes.

4. Damage prognostics

Prognostics is a new dynamically rising field where researchers utilize SHM data, machine learning algorithms and probabilistic modeling aiming to provide estimations for the future condition of a composite structure. They focus their efforts on the predictions of remaining useful life (RUL) and residual strength and they design prognostic frameworks with the capability to perform analysis in real-time. In order to succeed that, the availability of online SHM data is essential and AE is good candidate that fulfills this requirement.

Nevertheless, the literature review reveals that there is a limited number of papers published in the prognostics field where the researchers utilize AE data. The papers published in this field can be divided into the three groups, based on the models the authors adopt in order to perform predictions: regression analysis, artificial neural network (ANN) and hidden Markov-based models. The details of the studies focused on the prognostics of laminated composites using AE are presented in Table 6.

The first group of literature used a linear or non-linear regression analysis to find a mathematical correlation between a special AE indicator and a mechanical property of the composite structures, mostly strength and RUL. Then, the mathematical model is used to extrapolate the mechanical properties of the structure in the future using the AE data of the structure. Philippidis and Assimakopoulou [130] used a non-linear data fitting to formulate a regression model between the AE counts and the residual strength of glass/epoxy coupons which were subjected to the constant and variable amplitude fatigue load. Then, they used the model to predict the residual strength of two new specimens: one with a different matrix material but under the same loading conditions as the previous ones and the other one with the same matrix but subjected to a new variable-amplitude fatigue load. The average

Table 6
Prognostics of mechanical properties of laminated composites using AE data.

Composites	Type of the test	SHM techniques	Prognostic methods	Utilized AE parameters	Predicted parameter	Approach	Ref.
Regression							
Glass/ epoxy	Quasi-static tensile after fatigue aging	AE	Regression	Cumulative counts	Tensile residual strength	By fitting a curve to the cumulative AE counts and residual strength, an empirical model was generated to predict the residual strength	[130]
Glass/ epoxy	Four-point bending fatigue test	AE	Regression	Cumulative counts	Flexural residual strength	By fitting a curve to the cumulative AE counts and residual strength an empirical model was generated to predict the residual strength	[131]
ANN							
Carbon/ epoxy	Quasi-static tensile test	AE	ANN	Amplitude	Failure Strength	Using the AE data collected up to 50% of failure load, the failure strength of coupons were predicted.	[132]
Glass/ epoxy	4 PB fatigue test	AE	ANN	Event counts	Flexural residual strength	GFRP specimens were pre-fatigued up to different portions of their fatigue life, then ANN was used to predict their residual strength	[136]
Carbon/ epoxy	Post-impacted tensile test	AE	ANN	Cumulative counts	Failure tensile load	The AE data collected to 50% and 75% of maximum load were used to train the ANN and then the ANN predicted the failure tensile load.	[133]
Glass/ epoxy	Compression after impact	AE	ANN	Counts, counts to peak, RMS and signal strength	Residual compression after impact strength	The AE data collected during the impact tests was used to train the ANN and then the ANN used to predict the impact damage tolerance	[137]
Glass/ epoxy	3 PB after aging	AE	ANN	Events, cumulative counts, cumulative energy, cumulative absolute energy, cumulative signal strength	Flexural failure strength	The specimens were aged for different times then the ANN with the AE data used to predict the flexural failure strength	[138]
Hidden Markov-based models							
Carbon/ epoxy	Open-hole fatigue tensile test	AE	NHHSMM	Windowed cumulative RA (rise time/amplitude	RUL	Using NHHSMM with AE data to predict RUL of CFRP specimens	[139]
Carbon/ epoxy	Open-hole fatigue tensile test	AE	NHHSMM and BNN	Windowed cumulative RA (rise time/amplitude	RUL	Comparing the performance of BNN and NHHSMM to predict RUL of CFRP specimens using the AE data	[134]
Carbon/ epoxy	Open-hole fatigue tensile test	AE+ DIC	NHHSMM	1/amplitude	RUL	Using NHHSMM to predict RUL of CFRP specimens using the fusion of AE data and DIC results	[135]

error of residual strength prediction for the coupon with the new loading condition and the coupon with new matrix material was 2.89% and 5.46% respectively. Caprino et al. [131] used an exponential regression model to correlate the 4 PB residual strength of pre-fatigued glass/epoxy composites to the total AE counts that had been recorded at the maximum stress level of the pre-fatigue tests.

The second group of researchers used ANN to predict the residual strength of pre-fatigued composite coupons based on their AE activities. The prediction process is usually done in two steps: first, the ANN is trained by the AE data collected from the already tested specimens and then, after the sufficient training, the ANN model is used to predict the degradation of the mechanical properties of a new coupon. Rajendraboopathy et al. [132] did the tensile test on 18 glass/epoxy specimens. They separated 12 specimens as the training set and used the collected AE data up to 30%, 40%, and 50% of the failure load. Afterward, this AE data and the corresponding maximum strength were used to train the ANN. After the training process, ANN was employed to predict the maximum strength of the 6 remained specimens based on their AE activities. The results showed the ANN that was trained with more data (AE data up to 50% of failure load) had a better prediction. Arumugam et al. [133] performed tensile tests on the low-velocity impacted carbon/epoxy laminates. They used the collected AE data up to 50% and 75% of the tensile failure load of the impacted specimens to train an ANN. Then, the trained model was used to predict the residual strength of some new samples with an error range of 0.4%–15%. They claimed that the proposed technique could predict the residual strength of impacted laminates just by loading them up to a percentage of their maximum load without inducing severe damages in them.

However, Loutas et al. [134] showed that the nonhomogeneous hidden semi Markov model (NHHSMM) could predict RUL of OHT carbon/epoxy specimens, subjected to the fatigue load, better than ANN, Bayesian neural networks (BNN) (see Fig. 8). They cited three reasons for the superiority of NHHSMM over BNN: 1) BNN works almost as a black box, 2) the oscillation of BNN predictions is much higher than NHHSMM, and 3) despite the claim of the aforementioned literature, the accuracy of BNN prediction is not improved by increasing the numbers of data, while the accuracy of NHHSMM is continually improved as more online AE data comes into play. Eleftheroglou et al. [135] used NHHSMM to predict RUL of the OHT coupons using a fusion of the AE and DIC data. The results showed that the accuracy of RUL prediction was improved considerably by data fusion in comparison with using the AE data individually.

5. Conclusions

This review addresses the employment of AE technique for damage characterization in laminated composites. The review was structured in two main sections: damage diagnostics and damage prognostics. A comprehensive damage diagnostic is usually done in three levels: damage initiation detection, damage identification and damage localization. Because damage localization was fully addressed in a recently-published review paper, it was not discussed here anymore. In the second section, three main prognostic approaches using the AE data were presented: regression models, ANN and hidden Markov-based models. The main conclusions of the review are listed hereafter:

- Most of AE features such as amplitude, energy, rise time, duration, counts, centroid frequency and peak frequency are highly affected by

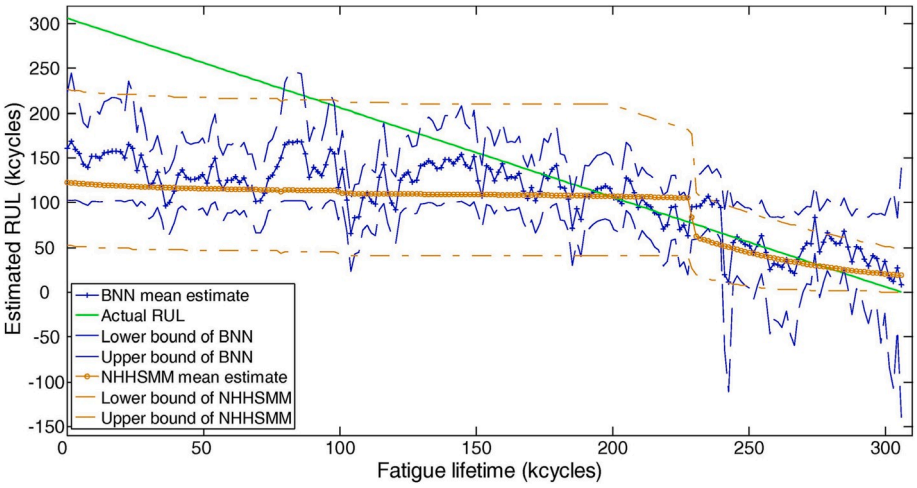

Fig. 8. RUL prognostic results for an OHT carbon/epoxy coupon using BNN and NHHSMM methods (lower and upper bounds shown for both models represent 90% confidence intervals) [134].

the sensor/source distance, sensor type, specimen's geometry and composite lay-up, coupling quality, damage state of the structure and user define parameters, i.e. threshold level, HDT and PDT parameters. These parameters should be taken into account to reach a reliable and robust AE monitoring of composite structures.

- The techniques that directly work with the AE waveform, such as Shannon's entropy and wavelet transform, can at least minimize the effect of threshold level and HDT and PDT parameters.
- Many researchers proposed the descriptive/qualitative criteria to detect the initiation of damage in laminated composites using AE that could result in different interpretations of damage initiation. Future work should be focused on the definition of some AE-based quantitative criteria for damage initiation detection tailored to the specific composite configurations. The historic index proposed by ASTM E2478-11 standard can be used as the foundation of future work.
- Different unsupervised clustering methods have been widely used for AE signals clusteting. The performance of these methods depends on the structure of the AE dataset. For example, for a simple AE dataset, k-means-based techniques, which are simple and fast, may work appropriately. While, for the reliable partitioning of a complicated AE dataset, hierarchical model, which has a higher computational cost, should be used. In addition, the repeatability of the clustering results should be evaluated.
- When a well-labeled training dataset is available, supervised classification techniques should be preferred over unsupervised clustering techniques to distinguish the complicated AE dataset meaningfully. Thus, it is recommended that the researchers create labeled-training dataset although it may requires extensive experimental campaigns.
- Prognostics is a new dynamically rising field, where researchers opt to predict the RUL and the strength of composite structure. In comparison with diagnostics-related literature, there is a limited number of papers where AE is utilized in order to provide the required input.
- The prognostics-related papers are categorized in three groups, based on the type of prediction models: regression models, neural networks-based models and hidden Markov-based models, which by moving from the first one to the last one, the complexity but also the reliability of the models increase.

Declaration of Competing interest

There is no conflict of interest.

References

[1] Yousefi J, Mohamadi R, Saeedifar M, Ahmadi M, Hosseini-Toudeshky H. Delamination characterization in composite laminates using acoustic emission features, micro visualization and finite element modeling. J Compos Mater 2015;50(22):3133–45.
[2] Mohammadi R, Saeedifar M, Toudeshky HH, Najafabadi MA, Fotouhi M. Prediction of delamination growth in carbon/epoxy composites using a novel acoustic emission-based approach. J Reinforc Plast Compos 2015;34(11):868–78.
[3] Saeedifar M, Fotouhi M, Najafabadi MA, Toudeshky HH. Interlaminar fracture toughness evaluation in glass/epoxy composites using acoustic emission and finite element methods. J Mater Eng Perform 2015;24(1):373–84.
[4] Roundi W, El Mahi A, El Gharad A, Rebiere J-L. Acoustic emission monitoring of damage progression in Glass/Epoxy composites during static and fatigue tensile tests. Appl Acoust 2018;132:124–34.
[5] Saeedifar M, Najafabadi MA, Zarouchas D, Toudeshky HH, Jalalvand M. Clustering of interlaminar and intralaminar damages in laminated composites under indentation loading using Acoustic Emission. Compos B Eng 2018;144:206–19.
[6] Malpot A, Touchard F, Bergamo S. An investigation of the influence of moisture on fatigue damage mechanisms in a woven glass-fibre-reinforced PA66 composite using acoustic emission and infrared thermography. Compos B Eng 2017;130:11–20.
[7] Yousefi J, Najfabadi MA, Toudeshky HH, Akhlaghi M. Damage evaluation of laminated composite material using a new acoustic emission Lamb-based and finite element techniques. Appl Compos Mater 2018;25(5):1021–40.
[8] Dionysopoulos D, Fierro G-PM, Meo M, Ciampa F. Imaging of barely visible impact damage on a composite panel using nonlinear wave modulation thermography. NDT E Int 2018;95:9–16.
[9] Dziendzikowski M, Kurnyta A, Dragan K, Klysz S, Leski A. In situ Barely Visible Impact Damage detection and localization for composite structures using surface mounted and embedded PZT transducers: a comparative study. Mech Syst Signal Process 2016;78:91–106.
[10] He Y, Tian G, Pan M, Chen D. Non-destructive testing of low-energy impact in CFRP laminates and interior defects in honeycomb sandwich using scanning pulsed eddy current. Compos B Eng 2014;59:196–203.
[11] Katunin A, Dragan K, Dziendzikowski M. Damage identification in aircraft composite structures: a case study using various non-destructive testing techniques. Compos Struct 2015;127:1–9.
[12] Klepka A, Pieczonka L, Staszewski WJ, Aymerich F. Impact damage detection in laminated composites by non-linear vibro-acoustic wave modulations. Compos B Eng 2014;65:99–108.
[13] Kudela P, Radzienski M, Ostachowicz W. Impact induced damage assessment by means of Lamb wave image processing. Mech Syst Signal Process 2018;102:23–36.
[14] Mustapha S, Ye L, Dong X, Alamdari MM. Evaluation of barely visible indentation damage (BVID) in CF/EP sandwich composites using guided wave signals. Mech Syst Signal Process 2016;76–77:497–517.
[15] Polimeno U, Meo M. Detecting barely visible impact damage detection on aircraft composites structures. Compos Struct 2009;91(4):398–402.
[16] Sikdar S, Kudela P, Radzieński M, Kundu A, Ostachowicz W. Online detection of barely visible low-speed impact damage in 3D-core sandwich composite structure. Compos Struct 2018;185:646–55.
[17] Toivola R, Lai P-N, Yang J, Jang S-H, Jen AKY, Flinn BD. Mechanochromic fluorescence in epoxy as a detection method for barely visible impact damage in CFRP composites. Compos Sci Technol 2017;139:74–82.

[18] Castellano A, Fraddosio A, Piccioni MD. Quantitative analysis of QSI and LVI damage in GFRP unidirectional composite laminates by a new ultrasonic approach. Compos B Eng 2018;151:106–17.
[19] Caminero MA, García-Moreno I, Rodríguez GP, Chacón JM. Internal damage evaluation of composite structures using phased array ultrasonic technique: impact damage assessment in CFRP and 3D printed reinforced composites. Compos B Eng 2019;165:131–42.
[20] Harizi W, Chaki S, Bourse G, Ourak M. Mechanical damage assessment of Polymer–Matrix Composites using active infrared thermography. Compos B Eng 2014;66:204–9.
[21] Li Y, Yang Z-w, Zhu J-t, Ming A-b, Zhang W, Zhang J-y. Investigation on the damage evolution in the impacted composite material based on active infrared thermography. NDT E Int 2016;83:114–22.
[22] Marani R, Palumbo D, Renò V, Galietti U, Stella E, D'Orazio T. Modeling and classification of defects in CFRP laminates by thermal non-destructive testing. Compos B Eng 2018;135:129–41.
[23] Hu H, Wang B-T, Lee C-H, Su J-S. Damage detection of surface cracks in composite laminates using modal analysis and strain energy method. Compos Struct 2006;74(4):399–405.
[24] Herman AP, Orifici AC, Mouritz AP. Vibration modal analysis of defects in composite T-stiffened panels. Compos Struct 2013;104:34–42.
[25] Zeng Z, Tian Q, Wang H, Jiao S, Li J. Testing of delamination in multidirectional carbon fiber reinforced polymer laminates using the vertical eddy current method. Compos Struct 2019;208:314–21.
[26] Tan KT, Watanabe N, Iwahori Y. X-ray radiography and micro-computed tomography examination of damage characteristics in stitched composites subjected to impact loading. Compos B Eng 2011;42(4):874–84.
[27] Ochôa P, Infante V, Silva JM, Groves RM. Detection of multiple low-energy impact damage in composite plates using Lamb wave techniques. Compos B Eng 2015;80:291–8.
[28] Saeedifar M, Mansvelder J, Mohammadi R, Zarouchas D. Using passive and active acoustic methods for impact damage assessment of composite structures. Compos Struct 2019;226:111252.
[29] Dong J, Locquet A, Declercq NF, Citrin DS. Polarization-resolved terahertz imaging of intra- and inter-laminar damages in hybrid fiber-reinforced composite laminate subject to low-velocity impact. Compos B Eng 2016;92:167–74.
[30] De Angelis G, Meo M, Almond DP, Pickering SG, Angioni SL. A new technique to detect defect size and depth in composite structures using digital shearography and unconstrained optimization. NDT E Int 2012;45(1):91–6.
[31] Newman JW. 7.13 shearography nondestructive testing of composites. In: Beaumont PWR, Zweben CH, editors. Comprehensive composite materials II. Oxford: Elsevier; 2018. p. 270–90.
[32] Grosse CU, Ohtsu M. Acoustic emission testing, basics for research- applications in civil engineerin. Springer-Verlag Berlin Heidelberg; 2008.
[33] Harizi W, Chaki S, Bourse G, Ourak M. Mechanical damage assessment of Glass Fiber-Reinforced Polymer composites using passive infrared thermography. Compos B Eng 2014;59:74–9.
[34] Hagemaier D, McFaul HJ, Moon D. Nondestructive testing of graphite fiber composite structures. In: Proceedings of National Aeronautic and Space Engineering and Manufacturing Meeting, Los Angeles, California, USA; 1970. October 5-9.
[35] Hagemaier D, McFaul HJ, Moon D. Nondestructive testing of graphite fiber composite structures. Mater. Eval. 1970:133.
[36] Shateri M, Ghaib M, Svecova D, Thomson D. On acoustic emission for damage detection and failure prediction in fiber reinforced polymer rods using pattern recognition analysis. Smart Mater Struct 2017;26(6):065023.
[37] Romhány G, Czigány T, Karger-Kocsis J. Failure assessment and evaluation of damage development and crack growth in polymer composites via localization of acoustic emission events: a review. Polym Rev 2017;57(3):397–439.
[38] Chou HY, Mouritz AP, Bannister MK, Bunsell AR. Acoustic emission analysis of composite pressure vessels under constant and cyclic pressure. Compos Appl Sci Manuf 2015;70:111–20.
[39] Pascoe JA, Zarouchas DS, Alderliesten RC, Benedictus R. Using acoustic emission to understand fatigue crack growth within a single load cycle. Eng Fract Mech 2018;194:281–300.
[40] Fotouhi M, Heidary H, Ahmadi M, Pashmforoush F. Characterization of composite materials damage under quasi-static three-point bending test using wavelet and fuzzy C-means clustering. J Compos Mater 2012;46(15):1795–808.
[41] Fotouhi M, Sadeghi S, Jalalvand M, Ahmadi M. Analysis of the damage mechanisms in mixed-mode delamination of laminated composites using acoustic emission data clustering. J Thermoplast Compos Mater 2015;30(3):318–40.
[42] Oskouei AR, Ahmadi M. Acoustic emission characteristics of mode I delamination in glass/polyester composites. J Compos Mater 2009;44(7):793–807.
[43] Lissek F, Haeger A, Knoblauch V, Hloch S, Pude F, Kaufeld M. Acoustic emission for interlaminar toughness testing of CFRP: evaluation of the crack growth due to burst analysis. Compos B Eng 2018;136:55–62.
[44] Nikbakht M, Yousefi J, Hosseini-Toudeshky H, Minak G. Delamination evaluation of composite laminates with different interface fiber orientations using acoustic emission features and micro visualization. Compos B Eng 2017;113:185–96.
[45] Cesari F, Dal Re V, Minak G, Zucchelli A. Damage and residual strength of laminated carbon–epoxy composite circular plates loaded at the centre. Compos Appl Sci Manuf 2007;38(4):1163–73.
[46] Refahi Oskouei A, Zucchelli A, Ahmadi M, Minak G. An integrated approach based on acoustic emission and mechanical information to evaluate the delamination fracture toughness at mode I in composite laminate. Mater Des 2011;32(3):1444–55.
[47] Minak G, Zucchelli A. Damage evaluation and residual strength prediction of CFRP laminates by means of acoustic emission techniques. In: Durand LP, editor. Composite materials research progres. New York: Nova Science Publishers Inc; 2008. p. 165–207.
[48] Khayal OMES. Literature review on imperfection of composite laminated plates. J. Microsc. Ultra. 2017;5(3):119–22.
[49] International A. Standard practice for determining damage-based design stress for glass fiber reinforced plastic (GFRP) materials using acoustic emission. West Conshohocken, PA: ASTM International; 2016. ASTM E2478-11.
[50] Hamstad MA, Downs KS. On characterization and location of acoustic emission sources in real size composite structures—a waveform study. J Acoust Emiss 1995;13:31–41.
[51] Kharrat M, Placet V, Ramasso E, Boubakar ML. Influence of damage accumulation under fatigue loading on the AE-based health assessment of composite materials: wave distortion and AE-features evolution as a function of damage level. Compos Appl Sci Manuf 2018;109:615–27.
[52] Chai M, Zhang Z, Duan Q. A new qualitative acoustic emission parameter based on Shannon's entropy for damage monitoring. Mech Syst Signal Process 2018;100:617–29.
[53] Fotouhi M, Belalpour Dastjerdi P, Ahmadi M. Acoustic emission based method to characterize glass/epoxy composite damages during 3-point bending test. Int J Mater Sci 2014;4(1):22–30.
[54] Fotouhi M, Saeedifar M, Sadeghi S, Ahmadi Najafabadi M, Minak G. Investigation of the damage mechanisms for mode I delamination growth in foam core sandwich composites using acoustic emission. Struct Health Monit 2015;14(3):265–80.
[55] Mahdian A, Yousefi J, Nazmdar M, Zarif Karimi N, Ahmadi M, Minak G. Damage evaluation of laminated composites under low-velocity impact tests using acoustic emission method. J Compos Mater 2016;51(4):479–90.
[56] Michalcová L, Kadlec M. Carbon/epoxy composite delamination analysis by acoustic emission method under various environmental conditions. Eng Fail Anal 2016;69:88–96.
[57] Mohan R, Prathap G. An acoustic emission energy analysis and its use to study damage in laminated composites. J Nondestr Eval 1980;1(4):225–33.
[58] Saeedifar M, Fotouhi M, Ahmadi Najafabadi M, Hosseini Toudeshky H. Prediction of delamination growth in laminated composites using acoustic emission and Cohesive Zone Modeling techniques. Compos Struct 2015;124:120–7.
[59] Heidary H, Ahmadi M, Rahimi A, Minak G. Wavelet-based acoustic emission characterization of residual strength of drilled composite materials. J Compos Mater 2012;47(23):2897–908.
[60] Nazmdar Shahri M, Yousefi J, Fotouhi M, Ahmadi Najfabadi M. Damage evaluation of composite materials using acoustic emission features and Hilbert transform. J Compos Mater 2015;50(14):1897–907.
[61] Pashmforoush F, Khamedi R, Fotouhi M, Hajikhani M, Ahmadi M. Damage classification of sandwich composites using acoustic emission technique and k-means genetic algorithm. J Nondestr Eval 2014;33(4):481–92.
[62] Hajikhani M, Ahmadi M, Farjpour M, Oskouei AR, Sharifi A. Strain energy release rate assessment in mode I delamination of foam core sandwich composites by acoustic emission. J Compos Mater 2011;45(22):2271–7.
[63] Fotouhi M, Najafabadi MA. Acoustic emission-based study to characterize the initiation of delamination in composite materials. J Thermoplast Compos Mater 2014;29(4):519–37.
[64] Fotouhi M, Suwarta P, Jalalvand M, Czel G, Wisnom MR. Detection of fibre fracture and ply fragmentation in thin-ply UD carbon/glass hybrid laminates using acoustic emission. Compos Appl Sci Manuf 2016;86:66–76.
[65] Barile C. Innovative mechanical characterization of CFRP by using acoustic emission technique. Eng Fract Mech 2019;210:414–21.
[66] Kumar CS, Arumugam V, Sajith S, Dhakal HN, John R. Acoustic emission characterisation of failure modes in hemp/epoxy and glass/epoxy composite laminates. J Nondestr Eval 2015;34(4):31.
[67] Fotouhi M, Ahmadi Najafabadi M. Investigation of the mixed-mode delamination in polymer-matrix composites using acoustic emission technique. J Reinforc Plast Compos 2014;33(19):1767–82.
[68] Fotouhi M, Pashmforoush F, Ahmadi M, Refahi Oskouei A. Monitoring the initiation and growth of delamination in composite materials using acoustic emission under quasi-static three-point bending test. J Reinforc Plast Compos 2011;30(17):1481.
[69] Saeedifar M, Fotouhi M, Ahmadi Najafabadi M, Hosseini Toudeshky H, Minak G. Prediction of quasi-static delamination onset and growth in laminated composites by acoustic emission. Compos B Eng 2016;85:113–22.
[70] Saeedifar M, Fotouhi M, Ahmadi Najafabadi M. Investigation of push-out delamination using cohesive zone modelling and acoustic emission technique. J Compos Mater 2015;50(25):3577–88.
[71] Sobhani A, Saeedifar M, Najafabadi MA, Fotouhi M, Zarouchas D. The study of buckling and post-buckling behavior of laminated composites consisting multiple delaminations using acoustic emission. Thin-Walled Struct 2018;127:145–56.
[72] Woo S-C, Kim T-W. High-strain-rate impact in Kevlar-woven composites and fracture analysis using acoustic emission. Compos B Eng 2014;60:125–36.
[73] Oz FE, Ersoy N, Lomov SV. Do high frequency acoustic emission events always represent fibre failure in CFRP laminates? Compos Appl Sci Manuf 2017;103:230–5.
[74] de Groot PJ, Wijnen PAM, Janssen RBF. Real-time frequency determination of acoustic emission for different fracture mechanisms in carbon/epoxy composites. Compos Sci Technol 1995;55(4):405–12.

[75] Gutkin R, Green CJ, Vangrattanachai S, Pinho ST, Robinson P, Curtis PT. On acoustic emission for failure investigation in CFRP: pattern recognition and peak frequency analyses. Mech Syst Signal Process 2011;25(4):1393–407.

[76] Saeedifar M, Saleh MN, De Freitas ST, Zarouchas D. Damage characterization of adhesively-bonded Bi-material joints using acoustic emission. Compos B Eng 2019;176:107356.

[77] Mohammadi R, Najafabadi MA, Saeedifar M, Yousefi J, Minak G. Correlation of acoustic emission with finite element predicted damages in open-hole tensile laminated composites. Compos B Eng 2017;108:427–35.

[78] Ali HQ, Tabrizi IE, Khan RMA, Tufani A, Yildiz M. Microscopic analysis of failure in woven carbon fabric laminates coupled with digital image correlation and acoustic emission. Compos Struct 2019:111515.

[79] Ben Ameur M, El Mahi A, Rebiere J-L, Gimenez I, Beyaoui M, Abdennadher M, et al. Investigation and identification of damage mechanisms of unidirectional carbon/flax hybrid composites using acoustic emission. Eng Fract Mech 2019;216:106511.

[80] Haggui M, El Mahi A, Jendli Z, Akrout A, Haddar M. Static and fatigue characterization of flax fiber reinforced thermoplastic composites by acoustic emission. Appl Acoust 2019;147:100–10.

[81] Saidane EH, Scida D, Pac M-J, Ayad R. Mode-I interlaminar fracture toughness of flax, glass and hybrid flax-glass fibre woven composites: failure mechanism evaluation using acoustic emission analysis. Polym Test 2019;75:246–53.

[82] Tabrizi IE, Kefal A, Zanjani JSM, Akalin C, Yildiz M. Experimental and numerical investigation on fracture behavior of glass/carbon fiber hybrid composites using acoustic emission method and refined zigzag theory. Compos Struct 2019;223:110971.

[83] Hartigan JA, Wong MA. Algorithm as 136: a K-means clustering algorithm. J. Roy. Stat. Soc. C Appl. Stat. 1979;28(1):100–8.

[84] Bezdek JC, Ehrlich R, Full W. FCM: the fuzzy c-means clustering algorithm. Comput Geosci 1984;10(2):191–203.

[85] Ding P, Li Q, Huang X. Classification of acoustic emission sources produced by carbon/epoxy composite based on support vector machine. IOP Conf Ser Mater Sci Eng 2015;87:012002.

[86] Saidane EH, Scida D, Assarar M, Ayad R. Damage mechanisms assessment of hybrid flax-glass fibre composites using acoustic emission. Compos Struct 2017;174:1–11.

[87] Marec A, Thomas JH, El Guerjouma R. Damage characterization of polymer-based composite materials: multivariable analysis and wavelet transform for clustering acoustic emission data. Mech Syst Signal Process 2008;22(6):1441–64.

[88] Refahi Oskouei A, Heidary H, Ahmadi M, Farajpur M. Unsupervised acoustic emission data clustering for the analysis of damage mechanisms in glass/polyester composites. Mater Des 2012;37:416–22.

[89] Bishop C. Pattern recognition and machine learning. New York: Springer-Verlag; 2006.

[90] Vesanto J, Alhoniemi E. Clustering of the self-organizing map. IEEE Trans Neural Network 2000;11(3):586–600.

[91] Murtagh F. A survey of recent advances in hierarchical clustering algorithms. Comput J 1983;26(4):354–9.

[92] Sawan HA, Walter ME, Marquette B. Unsupervised learning for classification of acoustic emission events from tensile and bending experiments with open-hole carbon fiber composite samples. Compos Sci Technol 2015;107:89–97.

[93] Wickerhauser MV. Adapted wavelet analysis from theory to software. CRC Press, Taylor and Francis Group; 1994.

[94] Soman KP, Ramachandran KI, Resmi NG. Insight into wavelets: from theory to practice. third ed. PHI Learning; 2010.

[95] Khamedi R, Abdi S, Ghorbani A, Ghiami A, Erden S. Damage characterization of carbon/epoxy composites using acoustic emission signals wavelet analysis. Compos Interfac 2019:1–14.

[96] Qi G, Barhorst A, Hashemi J, Kamala G. Discrete wavelet decomposition of acoustic emission signals from carbon-fiber-reinforced composites. Compos Sci Technol 1997;57(4):389–403.

[97] Saeedifar M, Najafabadi MA, Zarouchas D, Toudeshky HH, Jalalvand M. Barely visible impact damage assessment in laminated composites using acoustic emission. Compos B Eng 2018;152:180–92.

[98] Beheshtizadeh N, Mostafapour A. Processing of acoustic signals via wavelet & Choi - williams analysis in three-point bending load of carbon/epoxy and glass/epoxy composites. Ultrasonics 2017;79:1–8.

[99] Komai K, Minoshima K, Shibutani T. Investigations of the fracture mechanism of carbon/epoxy composites by AE signal analyses. JSME Int. J. Ser. 1 Solid Mech. Material 1991;34(3):381–8.

[100] Boominathan R, Arumugam V, Santulli C, Adhithya Plato Sidharth A, Anand Sankar R, Sridhar BTN. Acoustic emission characterization of the temperature effect on falling weight impact damage in carbon/epoxy laminates. Compos B Eng 2014;56:591–8.

[101] Ni Q-Q, Iwamoto M. Wavelet transform of acoustic emission signals in failure of model composites. Eng Fract Mech 2002;69(6):717–28.

[102] Nimdum P, Renard J. Use of acoustic emission to discriminate damage modes in carbon fibre reinforced epoxy laminate during tensile and buckling loading. In: Proceedings of ECCM 15 - 15th European conference on composite materials. Venise, Italy, conference 2012-06-24, conference; 2012. p. 8.

[103] Russell SS, Henneke EG. Signature analysis of acoustic emission from graphite/epoxy composites. Technical Report. NASA; 1977.

[104] Zhou W, Zhang P-f, Zhang Y-n. Acoustic emission based on cluster and sentry function to monitor tensile progressive damage of carbon fiber woven composites. Appl Sci 2018;8(11):2265.

[105] Li L, Swolfs Y, Straumit I, Yan X, Lomov SV. Cluster analysis of acoustic emission signals for 2D and 3D woven carbon fiber/epoxy composites. J Compos Mater 2015;50(14):1921–35.

[106] Ramirez-Jimenez CR, Papadakis N, Reynolds N, Gan TH, Purnell P, Pharaoh M. Identification of failure modes in glass/polypropylene composites by means of the primary frequency content of the acoustic emission event. Compos Sci Technol 2004;64(12):1819–27.

[107] Tang J, Soua S, Mares C, Gan T-H. A pattern recognition approach to acoustic emission data originating from fatigue of wind turbine blades. Sensors 2017;17(11).

[108] Li L, Lomov SV, Yan X. Correlation of acoustic emission with optically observed damage in a glass/epoxy woven laminate under tensile loading. Compos Struct 2015;123:45–53.

[109] Li L, Lomov SV, Yan X, Carvelli V. Cluster analysis of acoustic emission signals for 2D and 3D woven glass/epoxy composites. Compos Struct 2014;116:286–99.

[110] Jong HJ. Transverse cracking in a cross-ply composite laminate - detection in acoustic emission and source characterization. J Compos Mater 2005;40(1):37–69.

[111] Woo S-C, Kim T-W. High strain-rate failure in carbon/Kevlar hybrid woven composites via a novel SHPB-AE coupled test. Compos B Eng 2016;97:317–28.

[112] Bussiba A, Kupiec M, Ifergane S, Piat R, Böhlke T. Damage evolution and fracture events sequence in various composites by acoustic emission technique. Compos Sci Technol 2008;68(5):1144–55.

[113] Bourchak M, Farrow IR, Bond IP, Rowland CW, Menan F. Acoustic emission energy as a fatigue damage parameter for CFRP composites. Int J Fatig 2007;29(3):457–70.

[114] Liu PF, Chu JK, Liu YL, Zheng JY. A study on the failure mechanisms of carbon fiber/epoxy composite laminates using acoustic emission. Mater Des 2012;37:228–35.

[115] Kim S-T, Lee Y-T. Characteristics of damage and fracture process of carbon fiber reinforced plastic under loading-unloading test by using AE method. Mater Sci Eng, A 1997;234–236:322–6.

[116] Ceysson O, Salvia M, Vincent L. Damage mechanisms characterisation of carbon fibre/epoxy composite laminates by both electrical resistance measurements and acoustic emission analysis. Scripta Mater 1996;34(8):1273–80.

[117] Godin N, Huguet S, Gaertner R. Integration of the Kohonen's self-organising map and k-means algorithm for the segmentation of the AE data collected during tensile tests on cross-ply composites. NDT E Int 2005;38(4):299–309.

[118] Gong XL, Gong XJ, Laksimi A, Benzeggagh ML. Application of tsai-Wu criterion to notched and unnotched composite laminates under torque loading. J Compos Mater 2000;34(6):460–78.

[119] Chen O, Karandikar P, Takeda N, Kishi Rcast T. Acoustic emission characterization OF a glass-matrix composite. Nondestr Test Eval 1992;8–9(1–6):869–78.

[120] Kotsikos G, Evans JT, Gibson AG, Hale J. Use of acoustic emission to characterize corrosion fatigue damage accumulation in glass fiber reinforced polyester laminates. Polym Compos 1999;20(5):689–96.

[121] Barré S, Benzeggagh ML. On the use of acoustic emission to investigate damage mechanisms in glass-fibre-reinforced polypropylene. Compos Sci Technol 1994;52(3):369–76.

[122] Zhuang X, Yan X. Investigation of damage mechanisms in self-reinforced polyethylene composites by acoustic emission. Compos Sci Technol 2006;66(3):444–9.

[123] Quispitupa A, Shafiq B, Just F, Serrano D. Acoustic emission based tensile characteristics of sandwich composites. Compos B Eng 2004;35(6):563–71.

[124] Masmoudi S, El Mahi A, El Guerjouma R. Mechanical behaviour and health monitoring by acoustic emission of sandwich composite integrated by piezoelectric implant. Compos B Eng 2014;67:76–83.

[125] Zarouchas D, van Hemelrijck D. Mechanical characterization and damage assessment of thick adhesives for wind turbine blades using acoustic emission and digital image correlation techniques. J Adhes Sci Technol 2014;28(14–15):1500–16.

[126] Loutas TH, Kostopoulos V. Health monitoring of carbon/carbon, woven reinforced composites. Damage assessment by using advanced signal processing techniques. Part I: acoustic emission monitoring and damage mechanisms evolution. Compos Sci Technol 2009;69(2):265–72.

[127] Loutas TH, Kostopoulos V, Ramirez-Jimenez C, Pharaoh M. Damage evolution in center-holed glass/polyester composites under quasi-static loading using time/frequency analysis of acoustic emission monitored waveforms. Compos Sci Technol 2006;66(10):1366–75.

[128] Hamdi SE, Le Duff A, Simon L, Plantier G, Sourice A, Feuilloy M. Acoustic emission pattern recognition approach based on Hilbert–Huang transform for structural health monitoring in polymer-composite materials. Appl Acoust 2013;74(5):746–57.

[129] Al-Jumaili SK, Holford KM, Eaton MJ, McCrory JP, Pearson MR, Pullin R. Classification of acoustic emission data from buckling test of carbon fibre panel using unsupervised clustering techniques. Struct Health Monit 2014;14(3):241–51.

[130] Philippidis TP, Assimakopoulou TT. Using acoustic emission to assess shear strength degradation in FRP composites due to constant and variable amplitude fatigue loading. Compos Sci Technol 2008;68(3):840–7.

[131] Caprino G, Teti R, de Iorio I. Predicting residual strength of pre-fatigued glass fibre-reinforced plastic laminates through acoustic emission monitoring. Compos B Eng 2005;36(5):365–71.

[132] Rajendraboopathy S, Sasikumar T, Usha KM, Vasudev ES. Artificial neural network a tool for predicting failure strength of composite tensile coupons using acoustic emission technique. Int J Adv Manuf Technol 2009;44(3):399–404.
[133] Arumugam V, Shankar RN, Sridhar BTN, Stanley AJ. Ultimate strength prediction of carbon/epoxy tensile specimens from acoustic emission data. J Mater Sci Technol 2010;26(8):725–9.
[134] Loutas T, Eleftheroglou N, Zarouchas D. A data-driven probabilistic framework towards the in-situ prognostics of fatigue life of composites based on acoustic emission data. Compos Struct 2017;161:522–9.
[135] Eleftheroglou N, Zarouchas D, Loutas T, Alderliesten R, Benedictus R. Structural health monitoring data fusion for in-situ life prognosis of composite structures. Reliab Eng Syst Saf 2018;178:40–54.
[136] Leone C, Caprino G, de Iorio I. Interpreting acoustic emission signals by artificial neural networks to predict the residual strength of pre-fatigued GFRP laminates. Compos Sci Technol 2006;66(2):233–9.
[137] Ramasamy P, Sampathkumar S. Prediction of impact damage tolerance of drop impacted WGFRP composite by artificial neural network using acoustic emission parameters. Compos B Eng 2014;60:457–62.
[138] Suresh Kumar C, Arumugam V, Sengottuvelusamy R, Srinivasan S, Dhakal HN. Failure strength prediction of glass/epoxy composite laminates from acoustic emission parameters using artificial neural network. Appl Acoust 2017;115:32–41.
[139] Eleftheroglou N, Loutas T. Fatigue damage diagnostics and prognostics of composites utilizing structural health monitoring data and stochastic processes. Struct Health Monit 2016;15(4):473–88.